UNIVERSITY of CALIFORNIA
SANTA CRUZ

VARIABLE X-RAY ABSORPTION IN HIGH-MASS X-RAY BINARIES CYGNUS X-1 AND VELA X-1

A thesis submitted in partial satisfaction of the
requirements for the degree of

BACHELOR OF SCIENCE

in

PHYSICS

by

James F. Maduzia

June 6th, 2011

The thesis of James F. Maduzia is approved by:

Professor David Smith
Advisor

Professor Adriane Steinacker
Theses Coordinator

Professor David P. Belanger
Chair, Department of Physics

Abstract

Variable X-ray Absorption in High-Mass X-ray Binaries Cygnus X-1 and Vela X-1

by

James F. Maduzia

In this paper I have taken archival Rossi X-ray Timing Explorer data of Vela X-1 and Cygnus X-1 and analyzed short time scale variations in the hydrogen column density using X-ray spectroscopy. This results in the ability to model the density of the stellar wind along the line of sight of the telescope and plot it against the phase of the binary star system. Also computed are cross-correlations between key components of the X-ray spectrum such as absorption, power-law emission, and the iron fluorescence line. Vela X-1 is found to have a regular dependence of its absorption level with its phase and this is consistent with both models and other results in the literature. Cygnus X-1 is found to have a very inconsistent amount of absorption, which appears to generally be very low, but has increases preferentially around the superior conjunction of the black hole. An analysis of the relationship between the power-law and Gaussian emissions components was carried out to determine if there was a significant fluorescence echo in Cygnus X-1, but none was found to be statistically significant.

Contents

List of Figures

To

my parents and grandparents

Acknowledgements

I want to thank David Johnson, Lynn Delker, and John Rodriguez for their dedication to my mastery of calculus and introductory physics, without which I would not have been nearly as successful as a physics major as I have. I also want to thank David Smith for his guidance which allowed this work to be possible. Finally, a special thanks to Laurel Ruhlen for helping me learn tools needed for my research.

1 Introduction

1.1 X-ray Astronomy

Persistent X-ray sources outside of our solar system were unintentionally seen by some of the earliest outer-atmosphere X-ray detection missions. The first X-ray binary source was discovered accidentally by a mission launched to detect X-rays from flares in the Sun's corona that had been reflected by the Moon (Giacconi 1962). This entire experiment was no more advanced than a bank of Geiger counters strapped to the side of a sub-orbital sounding rocket. Only the most intense and persistent X-ray sources were found using these early methods which also included balloon based observations. Among the sources found during this era were Cygnus X-1 (Bowyer et al. 1965), a black hole (Webster & Murdin 1972; Bolton 1972a,b,1975) and Vela X-1 (Chodil et al. 1967), a neutron star pulsar (Forman et al. 1973) with a spin period of 282.8 seconds (McClintock et al. 1976). Since the launch of purpose-built X-ray astronomy satellites such as Uhuru in 1970, a significant population of persistent X-ray sources has been discovered throughout the Galaxy. The study of cosmic X-rays was, by this time, considered a mature branch of astronomy. Optical range measurements of these early X-ray sources have since confirmed that they are accompanied by main sequence stars (Bradt & McClintock 1983). Mass lost from this star, known as the companion, falls onto the accretor, a neutron star or a black hole known as the 'compact object'. The X-rays are created during this process as the material from the companion loses a significant amount of gravitational potential energy while accreting onto the extremely dense compact object. This

understanding of how a binary star system creates X-rays has led to a system of classifications based on the size of the companion star. These classifications attempt to provide a basic framework that accounts for the mass transfer parameters of the system in order to explain the X-ray emissions of the binary itself. Figure 1.1 shows the sizes of Cygnus X-1 and Vela X-1 with their orbits relative to the size of the Sun.

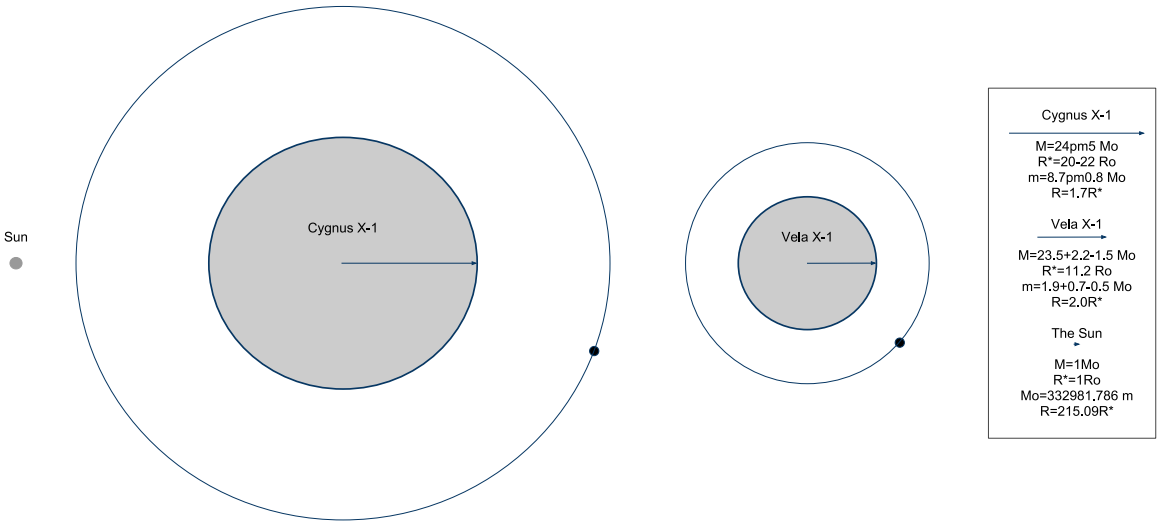

Figure 1.1: HMXB Orbital Scale Representations

1.2 Binary Star Systems

There are two significant mechanisms that allow mass transfer to occur between the members of a binary system. The first is known as Roche lobe overflow. This type of transfer happens when the tenuous outer layers of a companion star fall outside of its gravitational potential well and are then available for capture by the compact object. This results in a continuous accretion of stellar mass onto the compact object producing a steady source of X-rays. Roche Lobe accretion systems tend to be classified as Low Mass X-ray Binary (LMXB) systems. 'Low' refers to mass of companion star, which will be less than the mass of the compact object in the LMXB case. Here the companion star will appear to orbit the compact object while losing its outer layers to the compact object's

stronger gravitational potential as Roche Lobe overflow. The reason that LMXBs tend to fall into this classification is that heavier stars evolve faster and will reach their final state first, leaving the lighter star as the companion. The final state will be the neutron star or the black hole comprising the compact object.

Another mechanism for mass transfer is a stellar wind. A line-driven stellar wind occurs when black-body radiation emitted by the companion star is absorbed in the matching electronic energy levels of elements comprising the gas in the outer layers of the star. This process results in gas being emitted from the companion star's upper layers. Strong stellar winds are significant in young and super massive stars. It has been estimated that over the course of such a star's main sequence lifetime it can lose from $\frac{1}{4}$ to $\frac{1}{3}$ of its mass as a line-driven wind reaching speeds in the thousands of kilometers per second (Castor et al. 1975).

A very small fraction of this stellar wind can be captured by the compact object. To a first approximation, this can be modeled with a Bondi-Hoyle-Lyttelton (Hoyle & Lyttleton 1939 ; Bondi & Hoyle 1944) accretion geometry. This is where a star, moving supersonically through a uniform field of gas, gravitationally focuses the gas onto itself via an accretion column or 'wake'. However, for binary systems, there are many complications to this model that must be taken into account. For one, the velocity of the stellar wind is typically of the same order of magnitude as that of the compact object's orbital velocity. The orbit of the compact object also creates a consistent wake that perturbs the wind at all phase values (Theuns et al. 1996). Furthermore, there is a radiative feedback effect where X-rays from the accretion process interfere with the line-driven wind delivering the accretion material to the compact object (Blondin et al. 1990). There may also be a significant radiation pressure effect in the accretion column (Taam et al. 1991) along with other refinements to the original model including the gravitational 'drag' of the accretion column (Chandrasekhar 1943) and instabilities in the accretion flow (Cowie 1977).

Shown in Figure 1.2 are structures created by the interaction of the compact object's gravitational field with both the stellar wind and the outer layers of the companion star. The

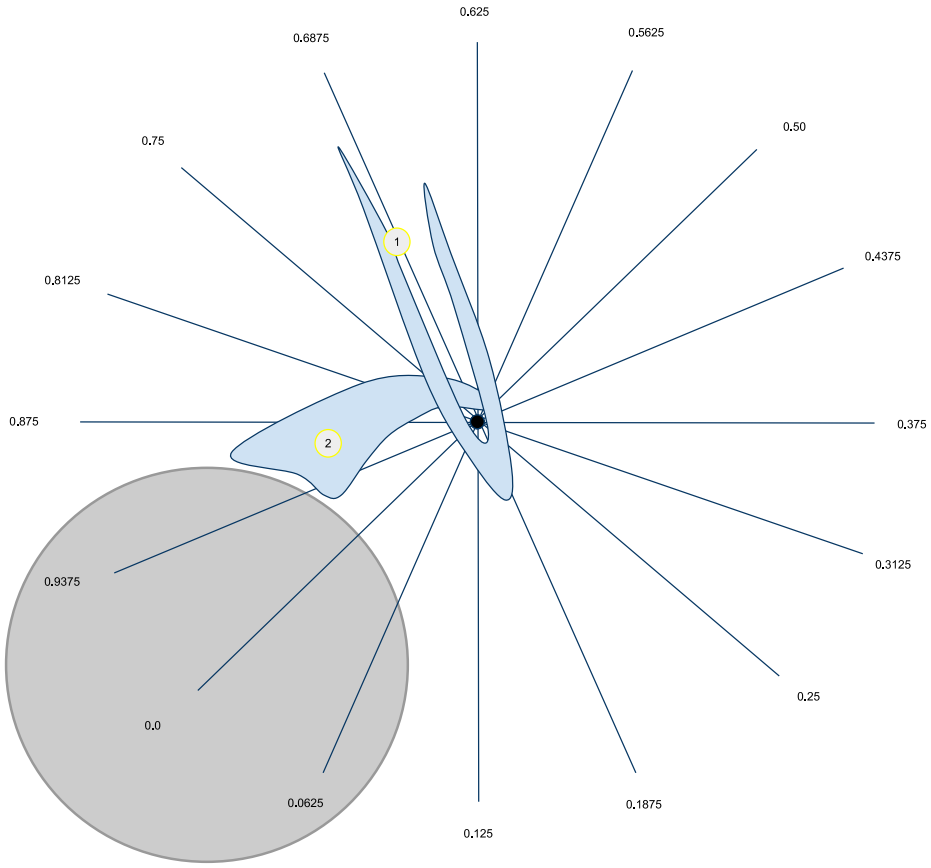

Figure 1.2: Theoretical Accretion Structures

figure is shown from the reference frame of the compact object in which the companion will spin and Earth will rotate around the binary system. The lines drawn on the figure show the path the X-rays must take to reach Earth at the given phase of the system. Structure 1 is the accretion wake which follows the path of the compact object and allows for accretion according to the Bondi-Hoyle-Lyttelton model. The structure labeled '2' is a representation of what is known as a tidal stream (Blondin et al. 1991) and a focused wind (Friend & Castor 1982).

Blondin's models show that a companion star, close to filling its Roche-lobe, may lose a steady stream of material to the compact object orbiting it closely. Due to the Coriolis effect, this tidal stream falls behind the compact object where it does not fully accrete. Due to this effect, the absorption measured in the system would increase disproportional to the luminosity. The models

have shown that while this process is highly sensitive to the orbital parameters of the compact object's orbit, it can have a significant effect even in a mostly wind-accreting system if the radius is small enough. It is most likely that the focused wind and the tidal stream form a single focusing structure which may vary in time.

Depending on the phase of the system, these absorption structures will greatly affect the amount of absorption seen by X-rays reaching Earth. This can be seen where the phase lines cross the structures in Figure 1.2. Not shown in the figure is the inclination angle. This is the angle that the orbital plane of the binary system makes with our perspective in observing. This angle would effect the absorption caused by these structures since they lie in the orbital plane. For Vela X-1 this angle is small enough to allow the neutron star to be eclipsed by it companion star. However, Cygnus X-1's inclination angle is too large for such an eclipse.

For wind accretion systems the compact object will often appear to orbit the companion since the companion star tends to be the more massive member in the binary. Such a system is classified as a High Mass X-ray Binary (HMXB), with 'high' once again referring to the size of the companion. Both Cygnus X-1 and Vela X-1 are classified as HMXBs.

As the stellar matter falls onto the compact object, it gives up its gravitational potential energy in the form of both radiation and internal kinetic energy. In order to produce the observed high-energy X-rays, the compact object must be one of the densest objects known in the universe, possessing a strong potential well. This gravitational potential energy is converted into radiation in a number of ways. As the stellar material falls towards the compact object it must loose angular momentum in order to be accreted. This necessitates the formation of an accretion disk around the compact object (Shakura & Sunyaev 1973). As the gas becomes compacted in the ever increasing gravitational field of the compact object it begins to differentially spiral in, with the outer layers moving slowly and the inner region orbiting much faster. This differential motion results in the accreted material both losing angular velocity and heating up due to its viscosity. Depending on the strength of the gravitational attraction, the temperature in the disk can reach up to millions of kelvin

(Shapiro, Lightman, & Eardley 1976). The exact temperature that an accretion disk can reach is not known as the structure of the accretion disk itself is not yet fully understood and has in many cases been shown to vary inexplicably in time. The high temperatures found in the accretion disk result in thermal black-body X-ray radiation of the disk material from free-free electron interactions. This is the acceleration of the charged particles in the plasma of the disk, typically electrons scattering from ions.

The radiative energy created by an accretion process is not insignificant if the accretor possesses a strong enough gravitational pull. For a Schwarzschild black hole accreting via a Roche-lobe-fed accretion disk, the energy radiated can be 5% of the rest mass of the accreted material. For a Kerr black hole, depending on its angular momentum, this figure can surpass 40% (McClintock & Remillard 2004). This means that accretion-fueled radiation can be more efficient than nuclear fusion which can only reach roughly 0.3% efficiency in converting matter to energy. This makes accretion one of most efficient methods of energy conversion in the universe.

While most of Cygnus X-1's X-rays are originally created by its accretion disk, this thermal black-body emission is not seen in our spectra of the system. This is due to the re-processing of these X-ray photons by inverse Compton scattering in the corona of the black hole. A black hole's corona is a region of energetic electrons found outside of the event horizon and around the accretion disk. The exact source of the corona is unknown, but one explanation is that it has its origin in magnetic field loops created by internal magneto-hydrodynamic instabilities within the accretion disk (Stella & Rosner 1984). These magnetic field loops extend outside of the disk while connecting to the disk at different points along its radius. Plasma can get caught up in these magnetic field loops as the accretion disk rotates, dragging the plasma they contain along with them. Since the rotation rate of the material in the accretion disk depends on its radius, the plasma connected to a particular magnetic loop can collide with that of another, shock heating the plasma to extreme temperatures. These energetic electrons will inverse-Compton scatter the thermal black-body X-rays created in the disk. Depending on the spectral state of the system, it is possible for the majority of all soft

X-rays created in the accretion disk to be upscattered into this X-ray regime which is modeled by the power-law component in our fit of Cygnus X-1. This is known as the hard spectral state of Cygnus X-1 and is the desired state for our absorption measurements.

It is interesting to note that an accretion disk, and corona are the only mechanisms available for a black hole to emit x-rays, as they are actually located outside of the event horizon. Another means of radiation available to a neutron star is that of bremsstrahlung radiation of ionized gas interacting directly with its surface. As stellar material attempts to accrete on to a neutron star with a magnetic field, it will be funneled in along the magnetic field lines because all material with velocity perpendicular to these field lines will be deflected. The funneled material meets the surface of the star at the magnetic poles. When this ionized material impacts the surface it undergoes a deceleration which causes the release of bremsstrahlung radiation. These two accretion points are the source of all X-rays from the surface of the neutron star. If the magnetic poles of the neutron star do not line up with its axis of rotation then, as the neutron star spins, these radiation sources on its surface will go in and out of our view on earth. This is a description of a neutron star pulsar and accounts for the spin-pulse period seen in Vela X-1's X-ray spectra.

One final aspect of binary star systems that must be discussed is that of the relationship between the initial X-rays created by the compact object and those they create via fluorescence in the energy levels of neutral or partially ionized stellar material near the system. When the initial X-rays from the compact object are incident on such material they will cause electrons bound in its orbitals to be ejected. When an electron from a higher orbital falls down to take its place a photon with energy equal to the difference in binding energy between the two orbitals is created. The particular lines that we tend to see are caused by a K-shell transition because the innermost electrons in iron which have the highest photoelectric cross-section to hard X-rays. The lines are slightly different depending on the amount of ionization of the iron atom. This process is known as X-ray fluorescence. One particular transition which is overwhelmingly seen in our X-ray band is that of the 6.4 keV k-shell transition from neutral. The energy lines due to ionized iron are slightly

higher.

Depending on the orientation of the system there will be a differing amount of time lag between these two X-ray components when viewed from our perspective. Should the compact object be in-between us and its companion then only the X-rays traveling away from us can cause fluorescence. This is because when the compact object is in this position, known as its inferior conjunction, the vast majority of the stellar material is behind it with respect to us. The time between these two components will therefore be much greater by the time they arrive at our observatory than if the compact object is behind its companion. In this position, known as the the superior conjunction of the compact object, the fluorescence component must not be deflected significantly from the original path of initial X-rays in order for both photons to be seen by us on Earth. It is for this reason that the time lag between the two X-ray sources should be less when the system is in this orientation.

1.3 Discovery of the SFXT

There have only been a few dozen persistent binary systems discovered since the early days of X-ray astronomy. Recently, however, through the use of the wide-field high-energy ESA INTEGRAL observatory, there has been a discovery of a significant population of a seemingly new type of system whose x-ray behavior can not yet be fully explained.

Known as the Super-giant Fast X-ray Transient (SFXT), this new type of source exhibits extended periods of X-ray quiescence punctuated by significant emissions in the X-ray band lasting on the timescale of days to hours (Romano et al. 2010). The first candidate for this system was discovered by Yamauchi et al. (1995) using ASCA, and its optical companion later identified by Coe et al. (1996). The second SFXT was discovered with the Rossi X-ray Timing Explorer (RXTE) by Smith et al. (1998) and its optical counterpart identified with Chandra (Smith et al. 2003). Before IBIS, sources exhibiting this behavior had rarely been seen before in the X-ray spectrum because their X-ray emissions were so infrequent and the field of view of available telescopes so narrow. The instruments on INTEGRAL can resolve a high-energy source to within 1' inside of its $30° X 30°$ field

of view, which gives it a distinct advantage in finding SFXTs.

The processes involved in creating these short X-ray bursts are not entirely understood. Due to their the dim and infrequent nature, SFXTs have up to this point been found predominately within our own quadrant of the Galaxy. It has been speculated however, that in the universe at large, there may be a significant population of SFXTs which outnumbers that of persistent HMXBs (Negueruela et al. 2006).

One explanation for the emissions of these sources is a inhomogeneous stellar wind. It has been shown theoretically by Owocki and Rybicki (1984) that a line-driven stellar wind is inherently unstable. This instability could cause the wind to develop structures of dense gas clouds traveling out from the star. These clouds, should they accrete onto the compact object, would directly influence the rate of its X-ray emissions.

A small outward velocity perturbation on a particle of gas close to the companion star can blue shift its absorption lines into a range opaque to higher energy photons. There is an abundance of these photons at this point as they have not been absorbed closer in to the star since they are energetic beyond resonance with the ambient stellar material. The absorption of these photons will further increase the particle's outward acceleration making it opaque to even more energetic radiation which continues the process. While this inner material is being continually accelerated out from the star, unperturbed wind further out receives significantly less acceleration due to it being in a radiation shadow as the radiation that it would have been sensitive to has already been absorbed. The result of this process is a substantial region of faster moving inner gas which collides with a region of slower gas further out. This results in complicated forward and reverse shock formations which increases the temperature of the gas due to colliding structures in the stellar wind (Owocki et al. 1988). Depending on their size, these dense pockets of gas might be completely or partially accreted relatively quickly by the compact object resulting in an X-ray burst.

Unlike SFXTs, many systems belonging to the HMXB classification have tended to be persistent sources of X-rays consistent with a continuous wind-fed accretion. The differences between

the observed behavior of the SFXT and the HMXB may be due many factors which are difficult to observe such as the magnetic field strength of the neutron star (Bozzo et al. 2008) and instabilities in the wind which may allow the X-ray source to encounter different stages of the shock process. Smith et al. (2006) have proposed that SFXTs are actually HMXBs and that there is a continuum of binary star systems between the two extremes.

1.4 Purpose

Using data taken from the Rossi X-ray timing Explorer over the past decade, goal of this research is to understand the stellar wind of the companion stars of two archetypal HMXBs. Specifically of interest is how this wind influences the creation and absorption of the X-rays originating in the system. This is an effort to identify evidence for 'clumps' in the stellar wind. The data I process from RXTE create a profile of the stellar wind between our perspective and the X-ray emitter by probing its X-ray emissions with X-ray spectroscopy. These clumps could be created by the orbital motion of the binary system influencing the stellar wind around it, or they can form due to instabilities inherent within the wind itself. Depending on their size, these dense regions or 'clumps' of gas might be completely or partially accreted by the compact object resulting in an X-ray burst. Another way that a clump might be identified is if there is an energy dependent dip in the spectrum affecting lower energy X-rays since the lower energy X-rays would be absorbed by a cloud further out while the higher energy ones would pass through. This would cause a hardening in the spectrum.

This research is also concerned with any relationship between these clumps of gas and the X-ray outbursts of the binary systems. One way this can be explored is by looking at the time lag correlation between the initial dominant X-ray emission, and with the softer Gaussian fluorescence line due to iron. Finding these correlation data of observations taken at different phase regions of the system will allow us to see a more detailed picture of the relationship between the X-ray components which may provide evidence for X-rays from the source stimulating the fluorescence in the structures

of gas around the system.

2 Analysis Procedures

I downloaded archival RXTE proportional counter array (PCA) data for Cygnus X-1 and Vela X-1 from the NASA HEASARC W3Browse database. The data for Cygnus X-1 were selected only from the system's hard-state. The reason for this is discussed in the data fitting section for Cygnus X-1. Vela X-1 data were not screened other than to select data observations that were long enough. This is necessary to maintain good counting statistics in Vela X-1 since it is a far dimmer source than Cygnus X-1 as well as to smooth out the regular X-ray variation of the pulsar spin period. All of the desired observation identification numbers for each system are put into a master list file to be accessed by the procedure scripts for each respective system.

Shown in Figure 2.1 is an overview flowchart of the process I used to obtain the data for this thesis. Individual steps of this flowchart will be covered in the rest of this section.

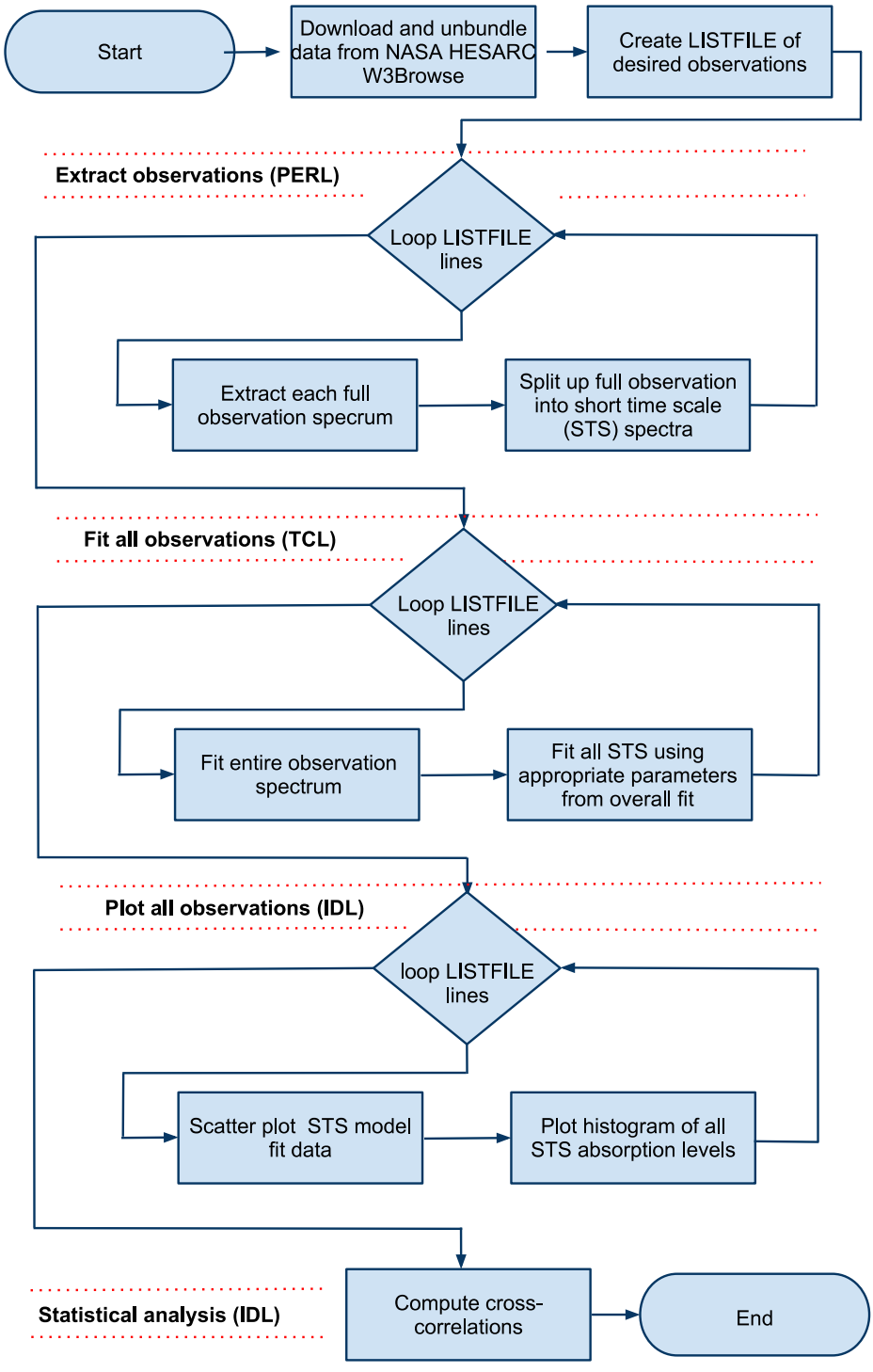

Figure 2.1: Analysis Procedure

2.1 Extraction

This initial part of the data procedure extracted data from all the observations with identification numbers given in the master list file. The extraction process was written entirely in PERL and uses the programs bundled in the FTOOLS 5.3 package. In the extraction process the program extracts a pulse height analyzer (PHA) spectrum for each desired observation ID in the list. Then it split this spectrum up into short timescale spectra (STS). For Cygnus X-1, each of these spectra were exposed for 16 seconds while for reasons mentioned before, those for Vela X-1 are exposed much longer. Since we used the standard mode 2 of the PCA we can only work with exposures with time bins in multiples of 16. In order to best match Vela X-1's spin period of 282.8 seconds I have alternated between two STS exposed for 288 seconds and one exposed for 272 seconds which gives an average exposure of all Vela X-1 STS spectra at approximately 282.6 seconds. This avoids a beat frequency in our fit values due to the pulsar spin period and mismatched time bins. This time resolution is used for all Vela X-1 time series data in this work. The data are also filtered out when ever the angle between the pointing direction of RXTE and the horizon of the earth, or the 'elevation angle' is less than 10°. Lastly, the data are screened out when RXTE is passing through the South Atlantic Anomaly.

2.2 Fitting

The program used to fit the extracted spectra is the XSPEC version 12.5.1 software. In my procedure it is controlled using the TCL scripting language. First, the entire spectra for each desired observation was fitted with all parameters allowed to vary. From this fitting, key parameters which were not expected to vary on short timescales were saved to be utilized later.

Next, all short timescale spectra (STS) corresponding to a overall observation spectra were looped through and fit to the same model as the overall spectra they were chopped up from. The relevant key parameters taken from the overall spectra were then frozen into these smaller fits. The

fit parameters from each of these small spectra were printed by row to text files which were then saved by observation identification number.

2.2.1 Modeling Cygnus X-1

In the Cygnus X-1 fit, the compound XSPEC model that was used was: $WABS*(Powerlaw+Gaussian)$. Each additive component (Powerlaw, Gaussian) models a different source of X-rays. The Wisconsin photo-electric cross-section (WABS) provides an allowance for photo-electric absorption of the X-rays by hydrogen and heavier elements. The WABS model consists of a parameter estimating the number of hydrogen atoms in the absorption column in units of 10^{22} atoms cm^{-2}. The power-law model in Cygnus X-1 is thought to measure the black-body photons originating in the accretion disk that are relativistically inverse-Compton scattered from energetic electrons in the high-energy corona of the black hole. The parameters of this model component are the power-law photon index, a measure of the hardness of the spectrum, and the normalization of its X-ray photons $keV^1cm^{-2}s^{-1}$ at 1 keV. The Gaussian model addresses the iron-line fluorescence as a Gaussian function with a location and width in energy as well as an X-ray normalization. Our Gaussian component is centered at 6.5 keV for the iron-line and the width and normalization is allowed to vary in the fits.

For the fit of the entire observation, all of these model components are free to vary. The power-law index and the Gaussian line width and energy components from this fit are frozen into the corresponding STS fits. In these fits, the number of hydrogen atoms, power-law and Gaussian normalizations are allowed to vary.

If Cygnus X-1 is in its soft-state, a large portion of its spectrum comes from its accretion disk while the the hard energy tail of the power-law is weakened. Emissions from the accretion disk would be modeled with a black-body component. The WABS component will fit the low-energy tail drop off of the spectra to find a measure the absorption as the lower energies are susceptible to absorption from neutral material. However, if the spectrum is dominated by the low-energy

black-body in the first place this will create a model parameter degeneracy in our overall fit. The fitting algorithm cannot tell the difference between a relatively strong black-body with considerable absorption from a weaker black-body with little absorption. This is because there are only a few degrees of freedom at the low-energy range where all the absorption takes place and where the black-body component is dominant. In the soft-state, this region contains most of the photon counts in the RXTE PCA. When the system is in the hard-state, the power-law component dominates over the entire length of the spectrum. This provides ample degrees of freedom at higher energies to fit the X-ray emission and leaving the lower energy bins to fit the absorption. This is why the hard-state must to study the variability of absorption.

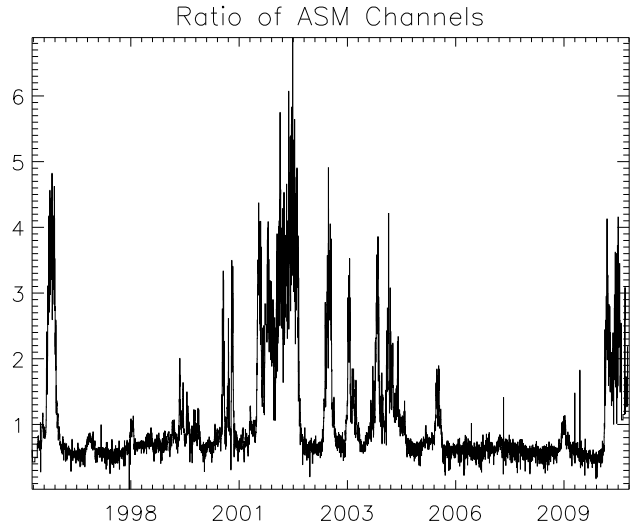

Figure 2.2: Cygnus X-1 ASM Energy Channel Ratio

The hard-state data are found by plotting the ratio of the RXTE All Sky Monitor (ASM) energy channels as A/(B+C) which is shown in Figure 2.2. The letters A,B, and C correspond to the three energy channels on the ASM which store photon counts seen within their energy band. The A band covers 1.5 - 3 keV, the B band covers 3 - 5 keV and the C band ranges from 5 to 10 keV. From this we can see that when the ratio is small there are more counts in the B and C bands and the system is in the hard-state. I selected data when this ratio was below 1.0 which signifies

that there are more counts in the B and C bands than the softer A band.

2.2.2 Modeling Vela X-1

The compound model used to fit Vela X-1 is: $WABS*(Bremsstrahlung+Gaussian)$. The bremstrahlung radiation model varies as the plasma temperature and a normalization. The Gaussian component, like in Cygnus X-1, gives a model of the iron fluorescence line that is prominent in the spectrum. As mentioned before, WABS provides a measurement of the photo-electric absorption.

The procedure for fitting Vela X-1's observations is the same as that used for Cygnus X-1. At first all parameters all allowed to vary in the fit of the entire observation. In the case of Vela X-1, the plasma temperature is frozen along with the Gaussian line and width for the STS fits.

2.2.3 Parameter Coupling in Correlations

For the spectra of each system, there is a very weak parameter degeneracy in effect that is very similar to the absorption and black-body component degeneracy which requires us to use hard-state data for Cygnus X-1. Although weak when seen individually, the process of adding up all of these individual orbit correlations into an overall average 'master' plot causes this coupling to become pronounced at the center time bin.

The strongest initial coupling is between the Gaussian normalization component and the absorption component since the ranges where they are most relevant overlap significantly. In this range it is possible to get a good fit for the data if both the Gaussian and the absorption fit values are both too high. This is because an increase in the absorption (which lowers the model) can be partially counteracted by an increase in the Gaussian normalization (which raises the model). Consequently, there can be many ways to get a correct fit to the spectra which may not be physical. As both of the components are high in this case the result is a positive correlation. The next step in this process is a correlation between the Gaussian and the power-law. This correlation is weaker since the ranges of these two components coincide less than before. If the power-law normalization goes

down then the Gaussian normalization must go up to compensate. This is a negative correlation.

Finally, notice that in this whole process if the absorption is high, then the Gaussian is high and the power-law is forced lower. However, if the absorption is too low then then the power-law must be high and the Gaussian low. Since the Gaussian is more strongly coupled to the absorption it acts as an intermediary between the absorption and the power-law. This is why the absorption and the power-law are very weakly coupled. All of the arguments concerning the parameter coupling only are significant for a correlation at no time lag. For any lag at all, these couplings are eliminated because there is no correlation whatsoever between completely different fits. Only the parameters taken and fit at the same time give a parameter degeneracy coupling. It is for this reason that the center points of my cross-correlations plotted in this paper are removed. In order to actually prove this conjecture I will need to use my whole process on data created by the XSPEC fakeit command and compare the results with the actual data.

2.3 Plotting

The same master list file that contains the desired observation numbers is read into IDL and looped over. For each of these observations the STS fit text file from the fitting procedure is read into IDL and its columns passed to IDL arrays. The time is read from the first column and is used to plot all of the model parameters against. Recall that each of the rows of these text files corresponds to a fit of a small timescale spectrum and the parameter uncertainties at the corresponding time. All of these fits are plotted separately for each observation. Each observation containing more than one orbit of RXTE has each individual orbit plotted separately along with the entire observation.

A two-dimensional histogram is created that plots the number of times a particular STS absorption fit value was detected at a particular phase for each binary system (Figures 3.8 and 4.8). The color denotes the number of times that a fit was detected while the x-axis location is its phase and the y-axis location is the amount of absorption. Red . Also, cross-correlations and auto-correlations of each individual observation are averaged around their midpoints to create a master

correlation plot. These are plotted in Figures 3.9 and 3.10 for Cygnus X-1. The figures created for Vela X-1 were not plotted due to that system's limited amount of data but will be discussed. Plots that directly compare the X-ray component correlations from Cygnus X-1 are plotted and shown in Figure 3.11. The correlations are created using the IDL routine 'C_correlate'. The time bin that corresponds to zero time lag is removed from all the correlation plots created. This is due to the parameter coupling between the parameters used to fit the systems which can result in a significant non-physical correlation at zero time lag.

3 Cygnus X-1 Results

3.1 Time variable fits

Featured in this section are plots of the hydrogen absorption and X-ray normalizations of Cygnus X-1 as a function of time. Each observation is plotted here with the data points being the parameter fits from the short timescale spectra. Only a small selection of all the processed observations are individually plotted and discussed here. They are chosen to show a wide range of behaviors seen in Cygnus X-1. Initially, an example of a common spectra to the system is shown, followed by an example of positively and negatively correlated time relationships between the absorption and the X-ray observations. Also featured here are observations that contain the maximum and minimum of all the fitted parameters seen in my data set. As mentioned before, the time resolution for Cygnus X-1 in these plots is 16 seconds. The plot for the absorption is plotted logarithmically while the X-ray normalizations have linear axes. Included in each plot is a figure that illustrates the approximate phase relationship between the members of the X-ray binary system at the time of emission of the spectrum featured in the observation.

The observation in Figure 3.1 exhibits behavior very common in Cygnus X-1 and is consistently seen at almost all phase values. This spectra is characterized by a randomly varying absorption at levels less than $1.375 * 10^{22} \frac{nH}{cm^2}$, a power-law normalization component of approximately 1.5 and a Gaussian normalization between 0.1 and 1.0. In these types of spectra there is little overall change in the parameters on the time scales of 20 minutes which is typical of the length of the RXTE orbits

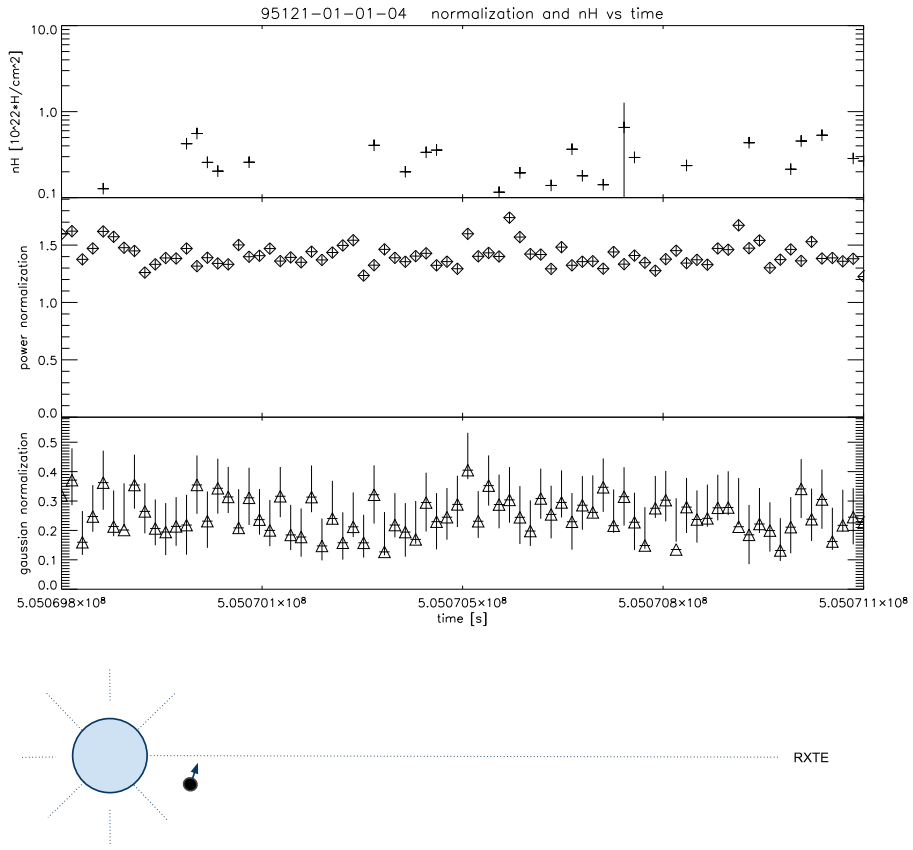

Figure 3.1: Typical Cygnus X-1 observation

shown in these observations.

The time series plot in Figure 3.2 was chosen as an example of anti-correlation between the hydrogen absorption and the X-ray emissions of the star. Notice that the X-ray normalization does not ever clearly jump up above its steadily rising baseline of emission rather it only dips below it as the absorption peaks. It is also important to note that these peaks in absorption occur when there is a relatively sparse overall hydrogen column density baseline. After the peaks, the absorption drops off to basically zero according to the fits. This observation occurs as the compact object is entering the last quarter of its orbit before reaching superior conjunction. It also occurs at the tail end of the region containing basically no fits above the baseline of absorption below $1.375 * 10^{22} \frac{nH}{cm^2}$. This is seen in Figure 3.8 roughly from phase 0.50 to 0.75. The power-law normalization here is slightly

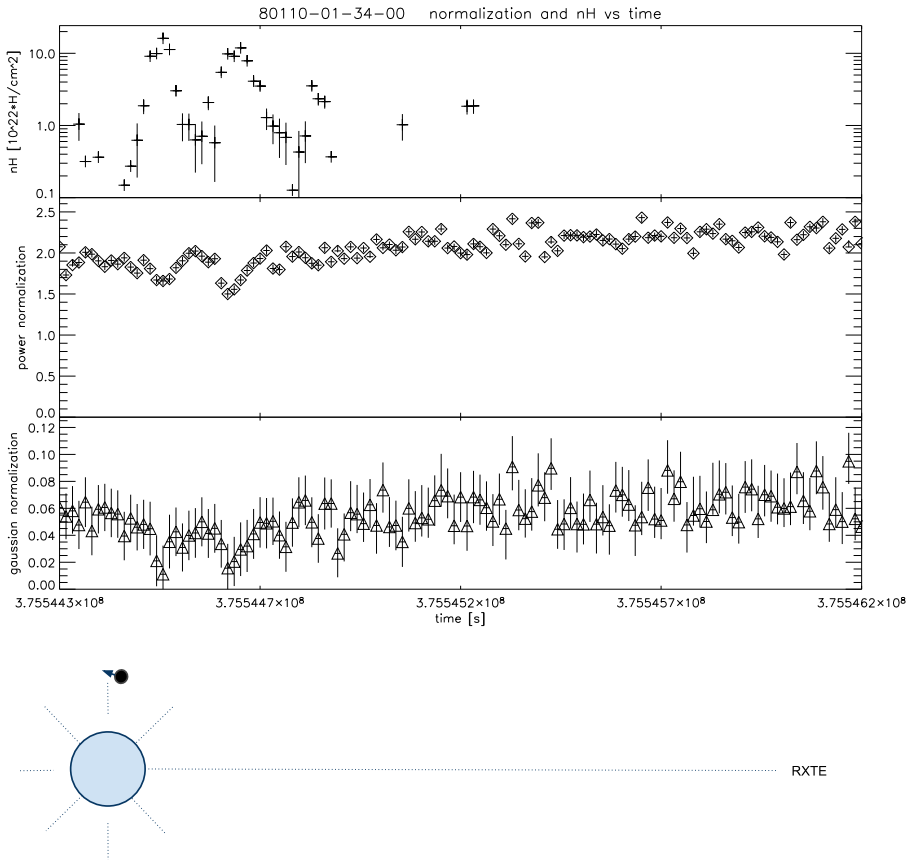

Figure 3.2: Anti-correlated Cygnus X-1 absorption and emission

higher than what is typically seen in this system at a normalization of 1.5. The Gaussian component in this observation is significantly less than the amount that is usually seen.

Figure 3.3 contains the observation with the highest absorption fits recorded in the data set. These peaks of absorption are found to be approximately ten times the absorption values than are typical for Cygnus X-1. Also unlike the absorption behavior typically seen in this system, this observation has significant absorption column variation on the scale of minutes. The absorption here varies from these rare and dense absorption fits to values much more sparse which are typically seen at all phases. This observation also shows the lowest power-law fits recorded in the data set used for this research at values consistently less than 1.0. The Gaussian component is an order of magnitude lower that where is it typically fit for this system. Finally, it should be noted that, by eye, it appears

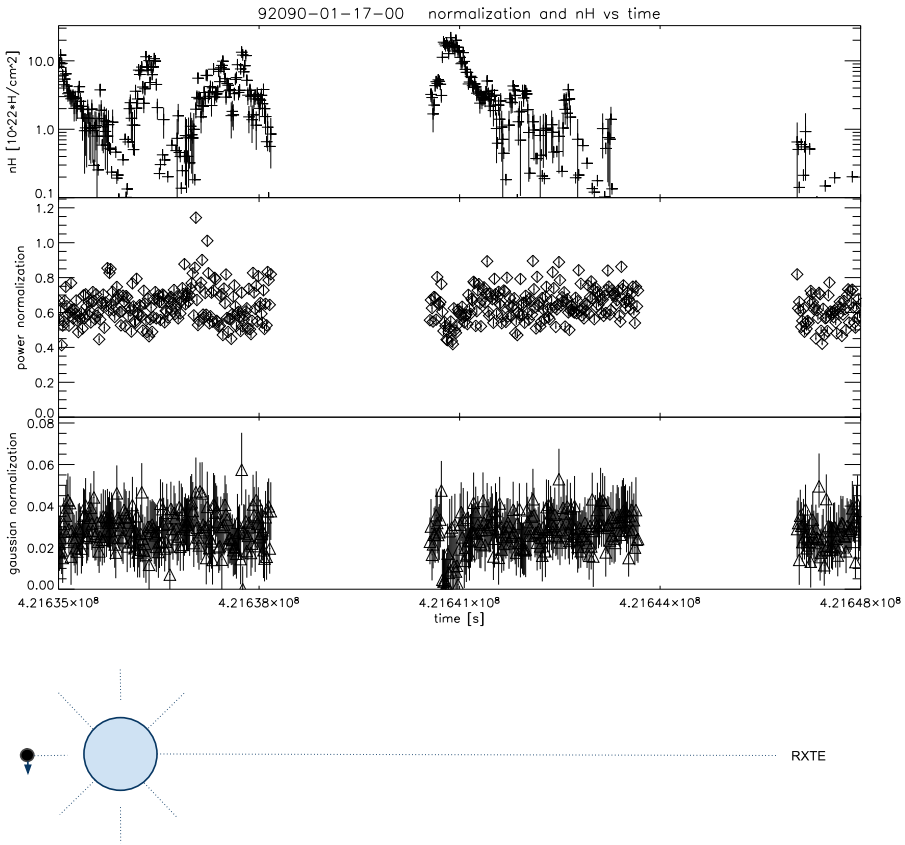

Figure 3.3: Maximum Cygnus X-1 absorption and minimum power-law normalization

that there appears to a very slight and irregular correlation between the absorption and the X-ray components here. In the first RXTE orbit, as the absorption rises and falls with almost no response from the X-ray normalizations other than a very few power-law fits that spike upwards. However, in the second orbit, there is an very large increase in density which clearly corresponds to a slight dip in the X-rays observed.

Figure 3.4 shows the least amount of absorption recorded of all the STS fits. This observation occurs when the black hole is approaching its superior conjunction, or its point furthest away from us as the observer. Although these just happen to be the smallest fits for the absorption, there are clearly instances in this observation, as well as of others typical of the system, that have fits of zero for the absorption. The power-law normalization shown here is also lightly lower than the

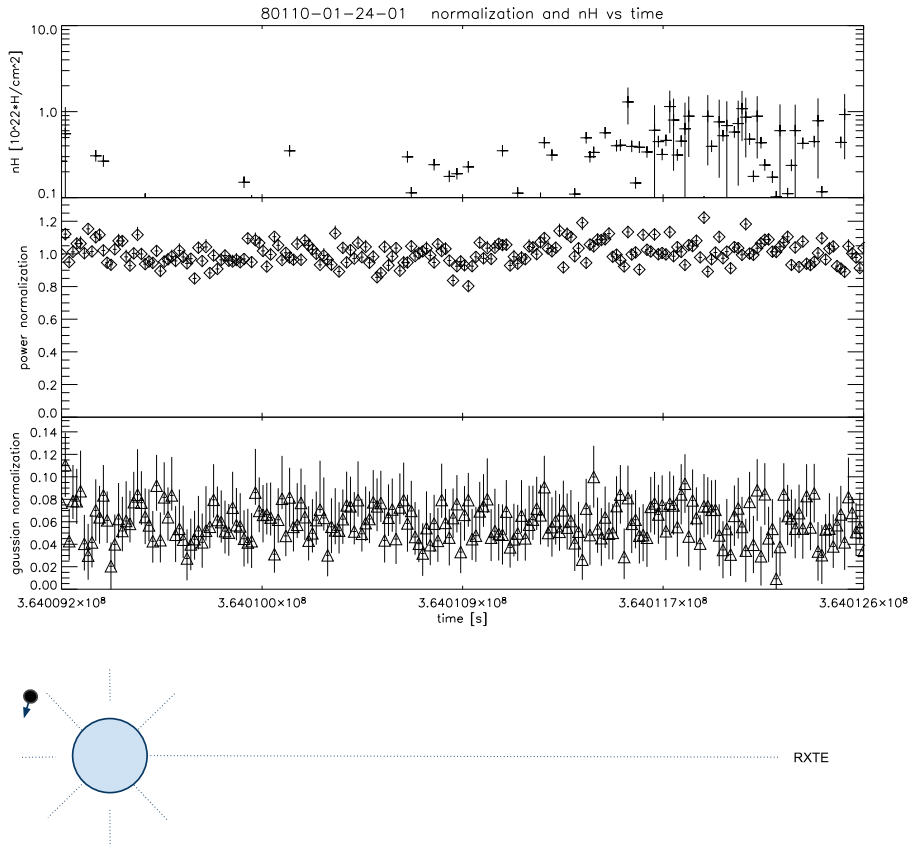

Figure 3.4: Minimum Cygnus X-1 absorption

typical value of 1.5. The Gaussian normalization is considerably lower than the usual amount seen.

Figure 3.5 shows the highest power-law normalizations found in the entire data set. These fits correspond to a higher than usual amount of Gaussian radiation. The amount of absorption in this particular observation is especially sparse, even for the values typically seen. There is a very steady rise in the power-law values over the course of this 30 minute observation, from about 2.0 to 2.5.

Figure 3.6 shows the highest Gaussian normalization recorded in the fits for this experiment. This is accompanied by slightly above average power-law radiation that is slowly decreasing in intensity over the course of the observation. Also notice that for most of this plot the absorption values are low. However, there are a few fits of the absorption early on that are about twice the

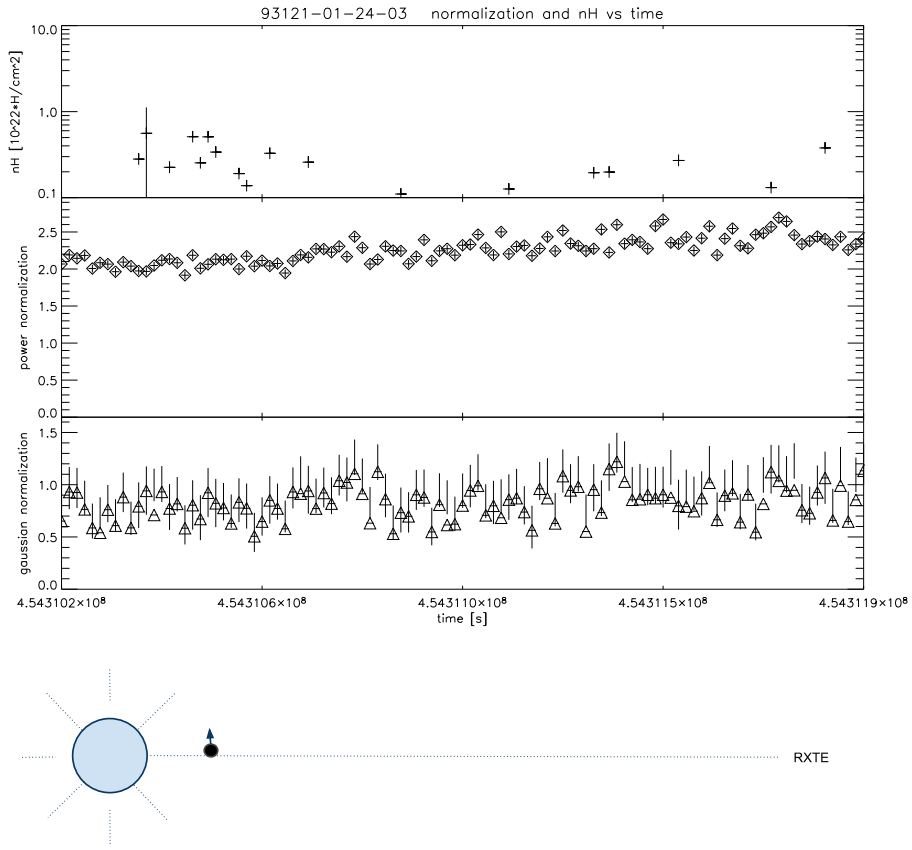

Figure 3.5: Maximum Cygnus X-1 power-law normalization

typical values. Also notice that there is a short time gap in the data sets in the middle of this observation.

Figure 3.7 shows the lowest Gaussian normalization recorded in the fits for this experiment. This is accompanied with typical values for the absorption column as well as lower than usual fits for the power-law component. Overall, the X-ray normalizations stay fairly flat over the course of this 20 minute observation.

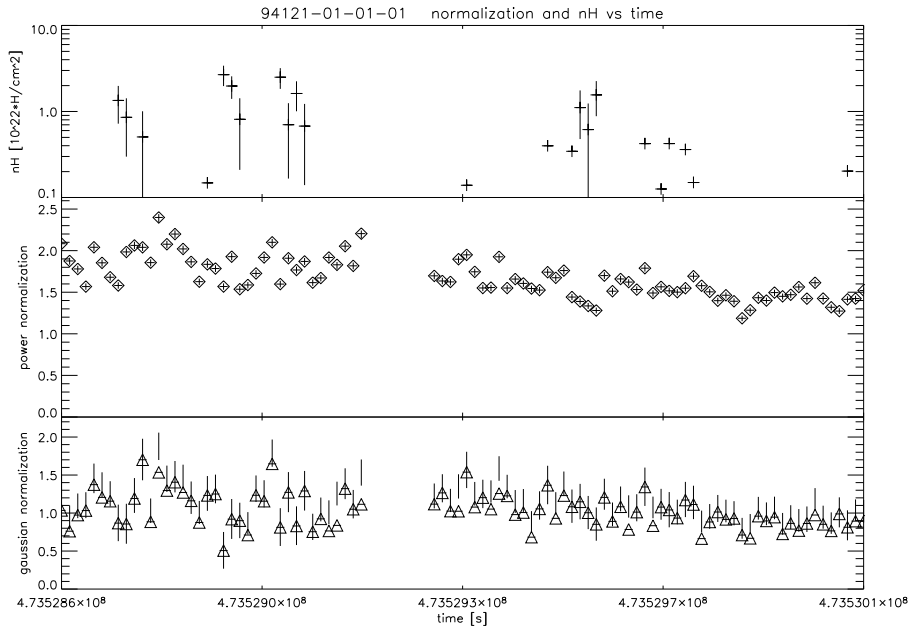

Figure 3.6: Maximum Cygnus X-1 Gaussian normalization

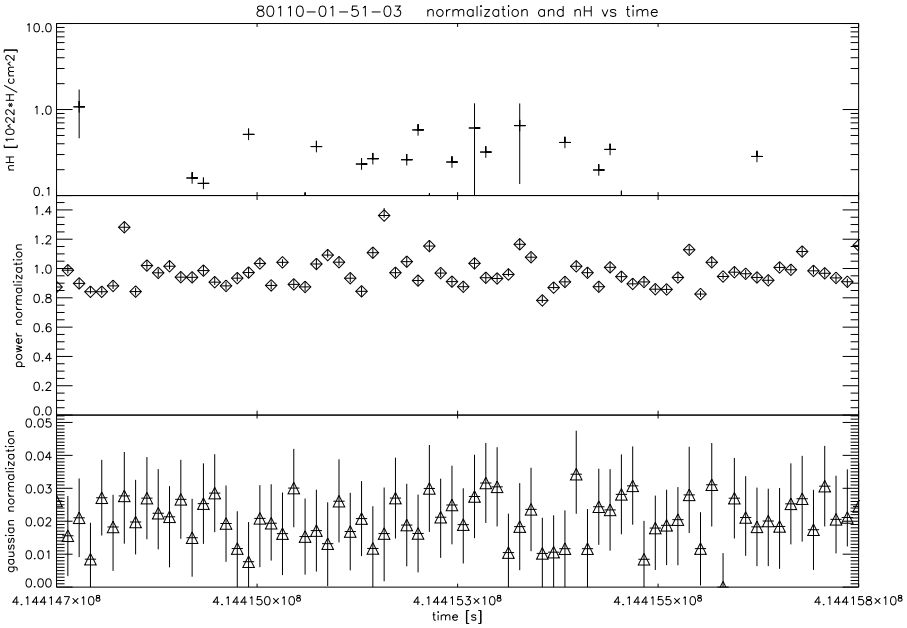

Figure 3.7: Minimum Cygnus X-1 Gaussian normalization

3.2 Absorption Histogram

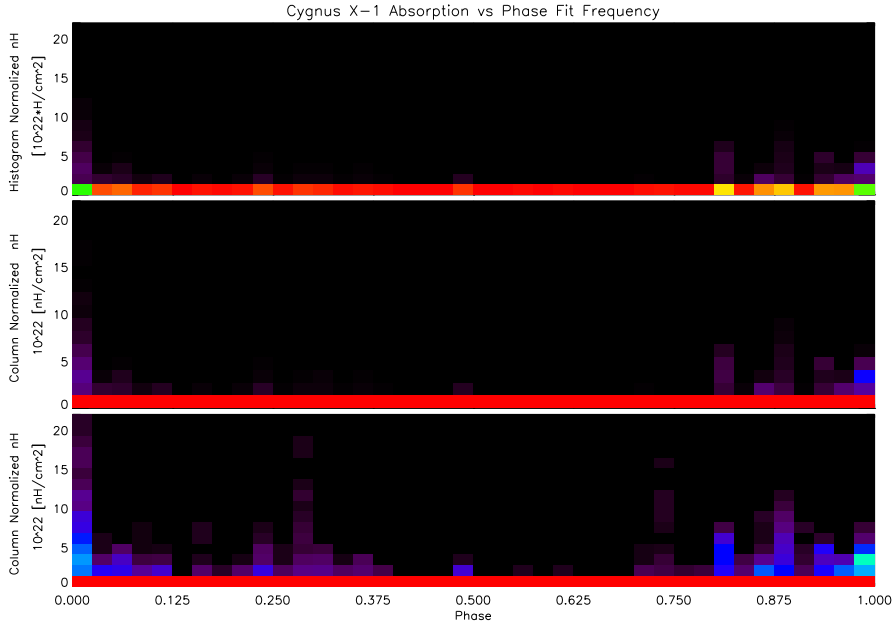

Figure 3.8: Cygnus X-1 phase-resolved absorption

The histogram featured in Figure 3.8 takes all of the STS and bins them appropriately according to their phase and absorption values. Red denotes a the largest number of data points while black is the absence of any at all. The top histogram in Figure 3.8 is histogram-wide normalized such that the data bin with the most counts out of the the entire histogram is marked in red and all the others are colored based on their relationship to this bin. In the lower two histograms, each column corresponding to a particular phase is normalized individually. That is, the data bin containing the most amount of points in each column is set to red and all other bins in that column are then colored relative to this bin. Finally, the difference between the second and third histograms is that the color numbering scheme is square-root normalized to emphasize the small amount of higher absorption fits found in the data.

At all orbital phases there is a very strong baseline of absorption less than $1.375 * 10^{22} \frac{nH}{cm^2}$ shown by the red count normalization at the base of the two 'column normalized' histograms at

the center and bottom of Figure 3.8. In general, when the black hole is in its superior conjunction there tends to be more high absorption fits measured. This is demonstrated in the top 'histogram normalized' histogram when the baseline deviates from a dense red color to a sparser yellow and green. The largest absorption peak is found at this phase. The absorption peaks seen at other phases in Figure 3.8 are typically only due to a small number of observations. Phases 0.125 to 0.50 denote a region where the low absorption dominates yet there are still a few random spikes to higher absorption values. After phase 0.5, there is a period of very low absorption below $1.375 * 10^{22} \frac{nH}{cm^2}$ with almost no fits above this value. This low absorption episode lasts until about phase 0.75. Starting here is a structure of several smaller peaks building back up to the largest peak at phase 1.0. While there are fits with absorption values up to 20 times the typical baseline fits, at all phases the system still has the majority of fits at a very low absorption values.

The root-normalized color scale absorption data in the third plot of Figure 3.8 show what looks like a large increase in the absorption column at phase 0.31. A closer look at the composition of this spike shows that the bin containing the highest peak of absorption at this phase (reaching over $1.0 * 10^{23} \frac{nH}{cm^2}$) is due to a single observation. Above $4.0 * 10^{22} \frac{nH}{cm^2}$, there are a total of 4 observations that contribute to this structure. These observations are from 2 consecutive years of RXTE data (2008 and 2009). This suggests that this structure may be a result of the orbital motion of the binary system but only because of a temporary state of the system.

Figures 3.9 and 3.10 show cross-correlations between the parameters of all available Cygnus X-1 data. For these plots all the correlations for each individual observation where were averaged together around their centers and then cut off at around 800 seconds. For the emission components there appears to be no correlation with the absorption whatsoever. Due to the parameter degeneracy coupling discussed in the plotting section, the data points in the center of the correlation, corresponding to no time lag, are removed.

In order to find any time lag relationship between the two emission parameters it is useful to compare the asymmetric nature of their cross correlation which is plotted in the bottom plot

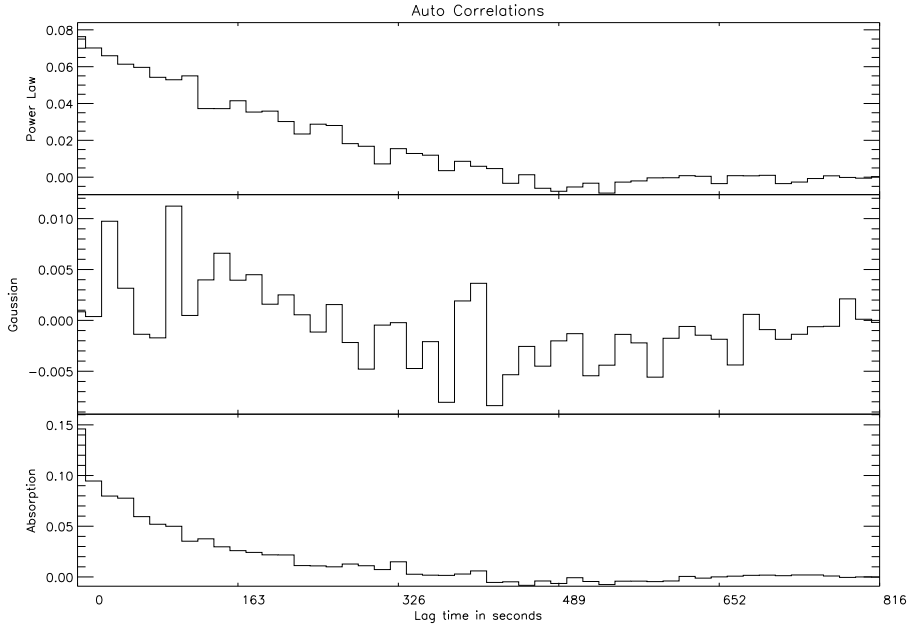

Figure 3.9: Cygnus X-1 Auto-Correlations

of 3.10. On the left side of this plot the Gaussian normalization component leads in time and on the right the power-law component leads in time. Figure 3.11 is the Gaussian leading side (red) folded over onto the power-law leading side (blue).

To get an idea of the relationship between the emission components of Cygnus X-1 at different phase orientations of the binary system, the correlation procedure which created Figure 3.11 is applied to data sets limited to the quarters of phase centered on the superior and inferior conjunction of the black hole. The superior conjunction set contains of all data between phase 0.875 and 1.125 and the inferior conjunction set contains all data located between phases 0.375 and 0.625. As done before, the left hand (Gaussian leading) side is folded over on to the power-law leading side. These two sets are plotted as before in Figures 3.12 and 3.13. These plots will give the amount of correlation between the components at time difference between the power law emission component and the fluorescence component. Since it is presumed that the secondary fluorescence component originates in the stellar wind and the power-law originates at the compact object, the time lag be-

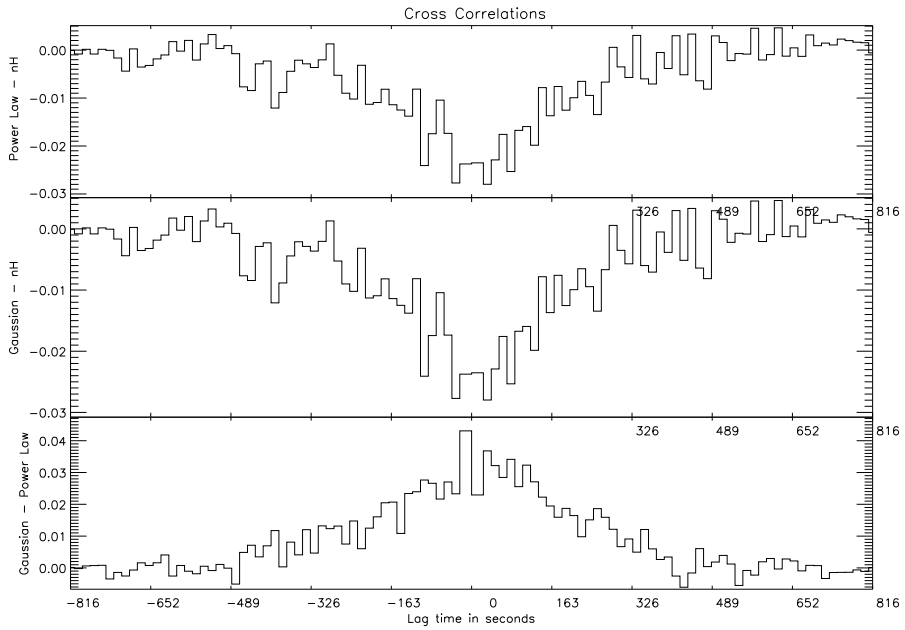

Figure 3.10: Cygnus X-1 Cross-Correlations

tween the components should in theory depend on the binary's phase location since that affects the travel time of the X-rays headed to our observatory.

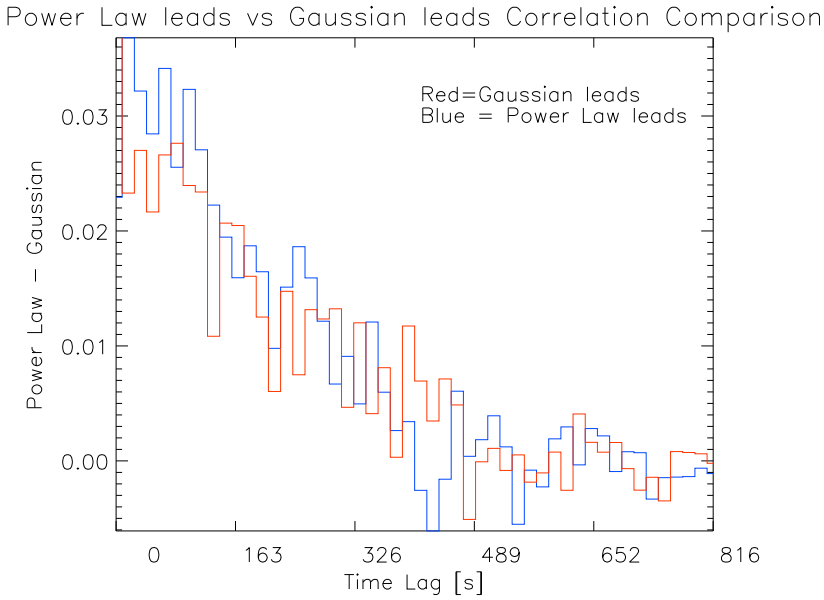

Figure 3.11: Full Cygnus X-1 data set

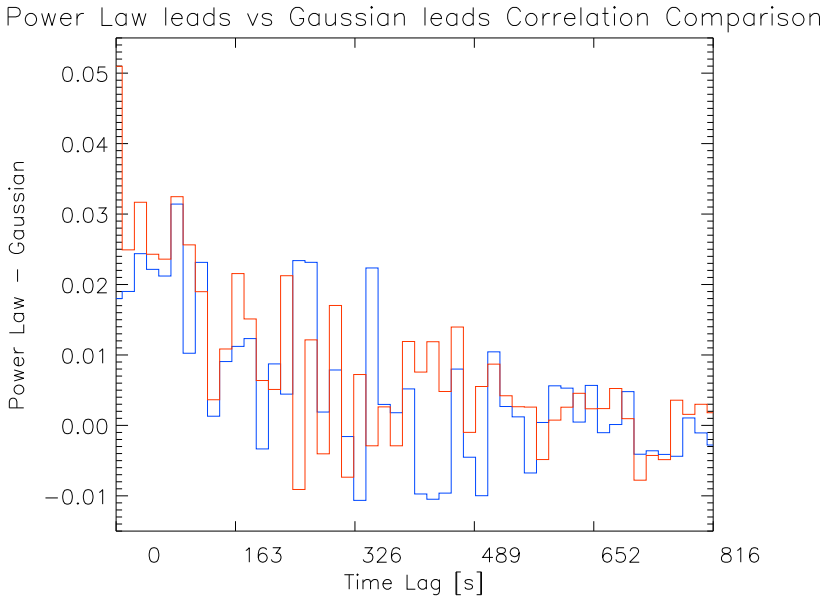

Figure 3.12: Inferior conjunction Cygnus X-1 data set

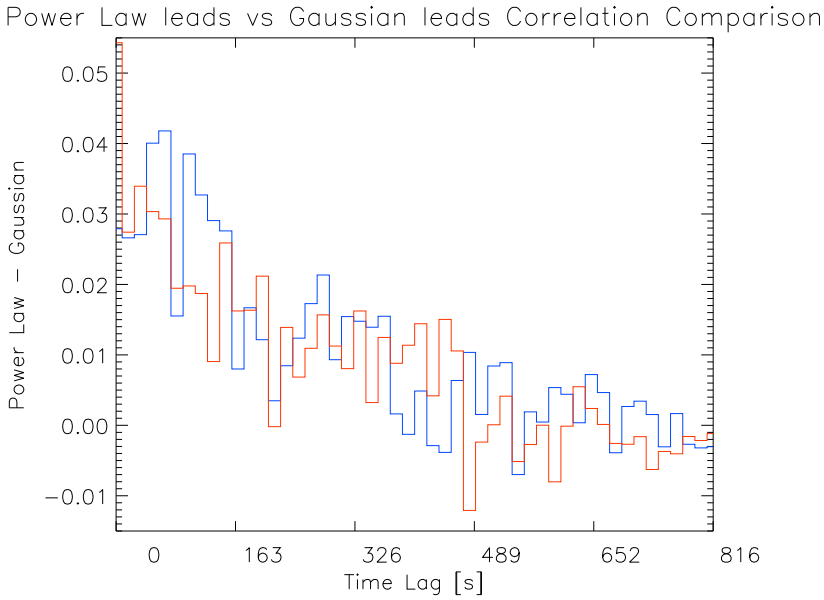

Figure 3.13: Superior conjunction Cygnus X-1 data set

4 Vela X-1 Results

4.1 Time variable fits

The spectrum of Vela X-1 is much more absorbed than that of Cygnus X-1. Rather than having a consistently low level of absorption with intermittent short increases, the absorption in Vela X-1 varies regularly with its phase. This variation is from less than $1.0 * 10^{23} \frac{nH}{cm^2}$ near the inferior conjunction of the neutron star up to $6.0 * 10^{23} \frac{nH}{cm^2}$ at higher phases of its orbit.

The observation shown in Figure 4.1 occurs at approximately phase 0.83 and it is about 850 seconds long. This observation contains the lowest value for the bremsstrahlung normalization for all of the Vela X-1 data that I have. In the observation, all three of the parameters are decreasing, although the X-ray parameters are falling off faster than the absorption. The absorption is low for the amount usually seen in this system at this phase, at $1.0 * 10^{23} \frac{nH}{cm^2}$. Each data point here corresponds to approximately the spin period of Vela X-1 at 282.8 seconds.

Observation 93039-01-01-11 (not shown) has the maximum value for the Gaussian normalization for all of the Vela X-1 data that I have. It is located at approximately 0.716 to 0.718 of phase and is also about 850 seconds long. This observation also has an absorption level typical of Vela X-1 at this phase, but like observation 10142-01-01-00 shown in Figure 4.1, it is too short to exhibit any meaningful time variation.

The Vela X-1 observation shown in Figure 4.2 is located just after the neutron star passes through its inferior conjunction (phase 0.5). The observation shows a consistently high absorption

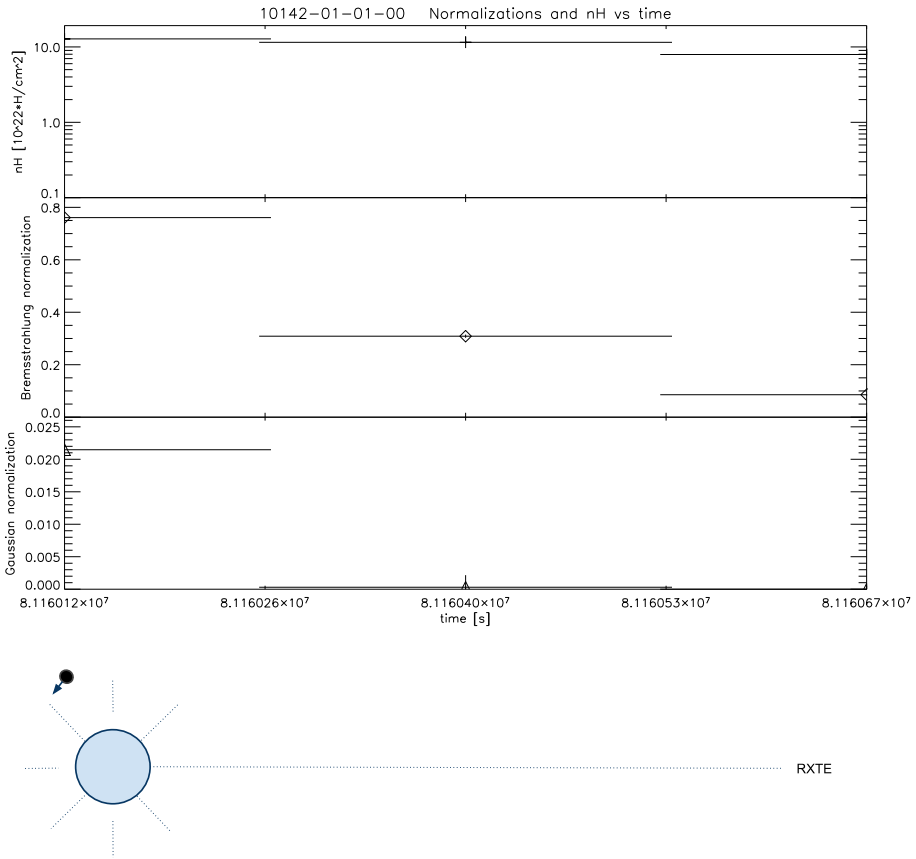

Figure 4.1: Minimum Vela X-1 bremsstrahlung normalization

level. The X-ray normalizations for both the bremsstrahlung and Gaussian components vary slightly but directly with each other.

Figure 4.3 shows what seems to be two particularly strong cases of anti-correlated behavior between the absorption and the X-ray normalization. Notice that at the end of the first orbit, when the absorption begins to drop off, the bremsstrahlung component of the X-rays increases dramatically. This happens again at the end of the third orbit. Overall, this observation has an entire order of magnitude less absorption than the previous observation discussed (Figure 4.2). The phase of this system is that of leaving egress and approaching the first quarter of phase. Notice that as a whole over the observation, all values are slowly declining. This observation has the least amount of absorption of all of the observations that I have processed.

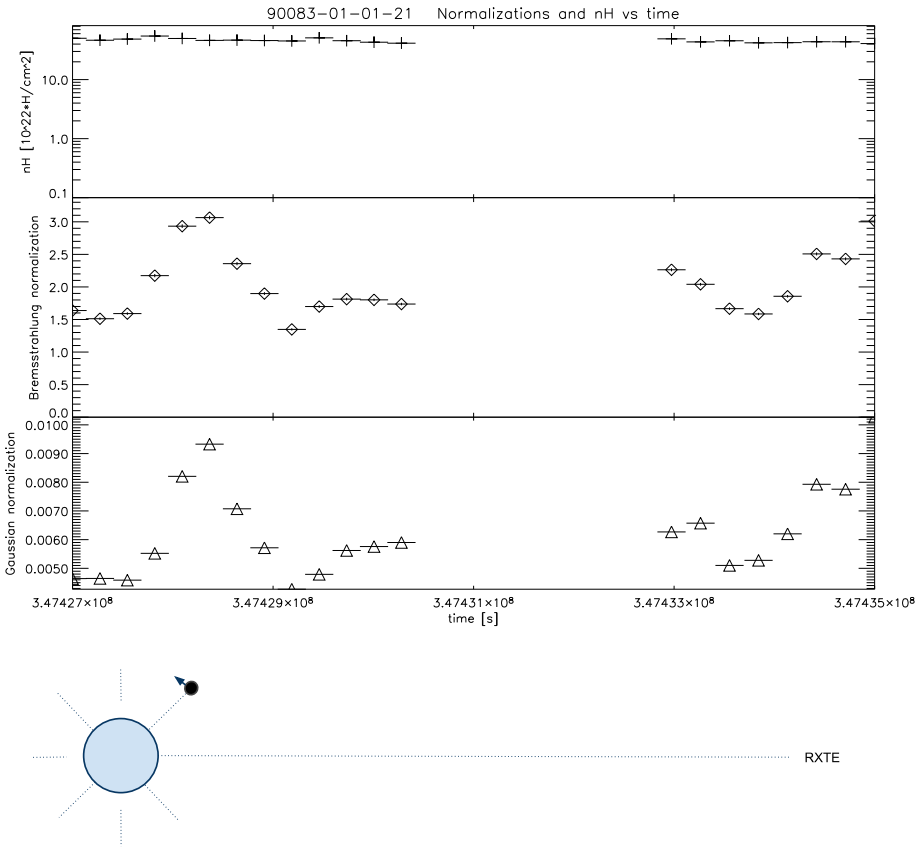

Figure 4.2: Vela X-1 X-ray variability

The observation in Figure 4.4, taken just before the neutron star eclipses, shows the baseline of X-ray emission to be steadily increasing while there is some variability in the emissions superimposed on it. The absorption appears to be relatively consistent. There is what looks to be a slight decrease in absorption as the X-ray intensity peaks in the third orbit.

The observation shown in Figure 4.5 occurs as soon after the neutron star has left eclipse. While they show some significant shorter term variability, the X-ray emissions of the source steadily increase over the observation until rapidly dropping off near the end. Throughout this time, the absorption is slowly but steadily declining. This observation has the highest value for the absorption column for all of the Vela X-1 data that I have.

This observation 4.6 has the highest value for the bremsstrahlung normalization for all

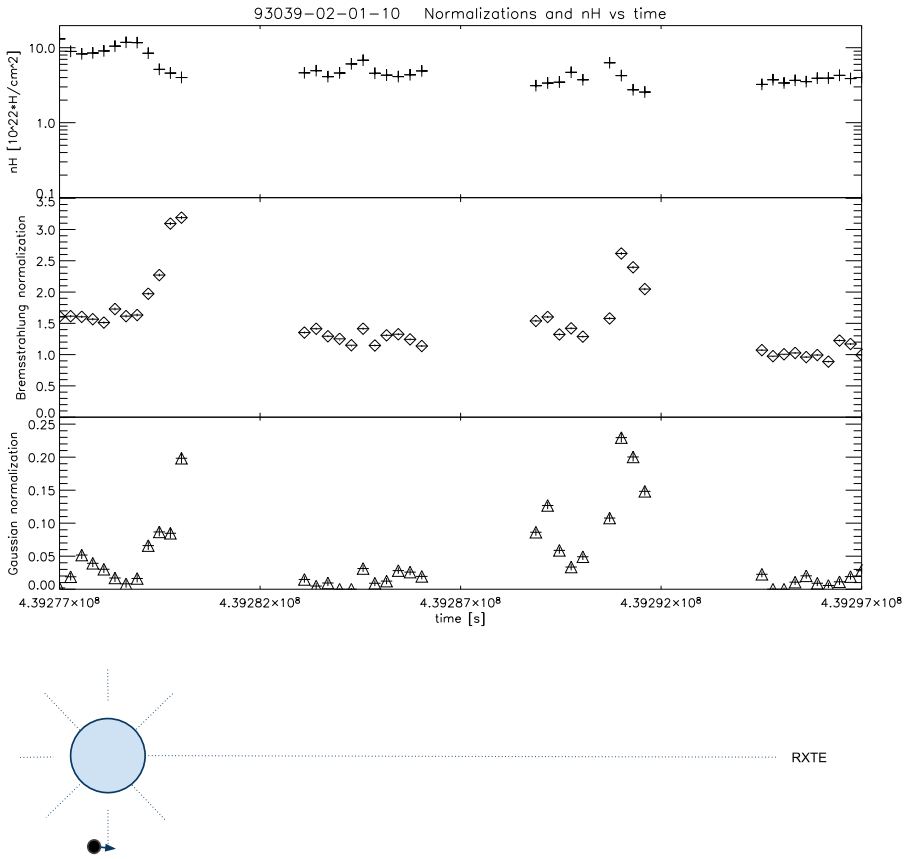

Figure 4.3: Anti-correlated Vela X-1 emissions and absorption

of the Vela X-1 data that I have. It also has levels of absorption that are roughly equal to that of the last observation, making them some of the highest recorded for this paper. Here the absorption stays relatively flat while the normalizations are quite variable. However, unlike other observations shown above, there is no overall trend of increasing or decreasing of the X-rays in the observation here. The Gaussian component and the bremsstrahlung component appear to be directly correlated in this observation. This particular observation is unique flare of Vela X-1 that occurred in RXTE year three (January 1998) and has not been observed since.

Figure 4.7 contains the minimum value for the Gaussian normalization for all of the Vela X-1 data that I have. This shows the absorption level staying steady at an amount that is a typical baseline for Vela X-1 while both of the X-ray components increase. After about 1200 seconds of both

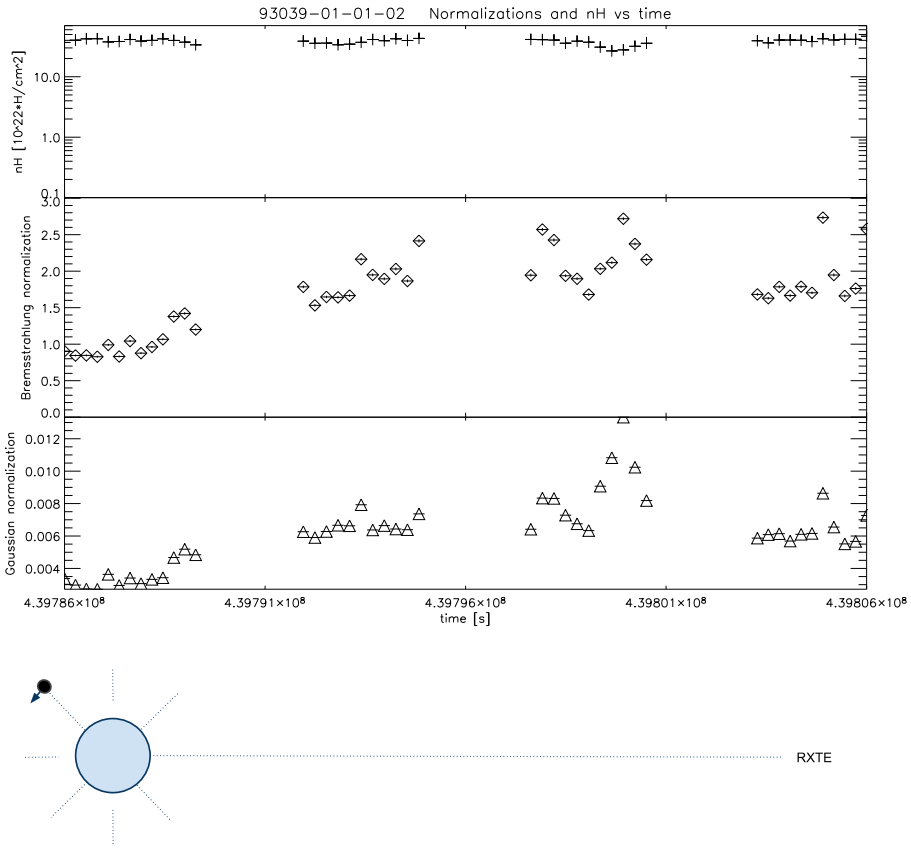

Figure 4.4: Vela X-1 increasing X-ray emissions

X-ray components increasing, the Gaussian component falls off, while the bremsstrahlung component continues to increase.

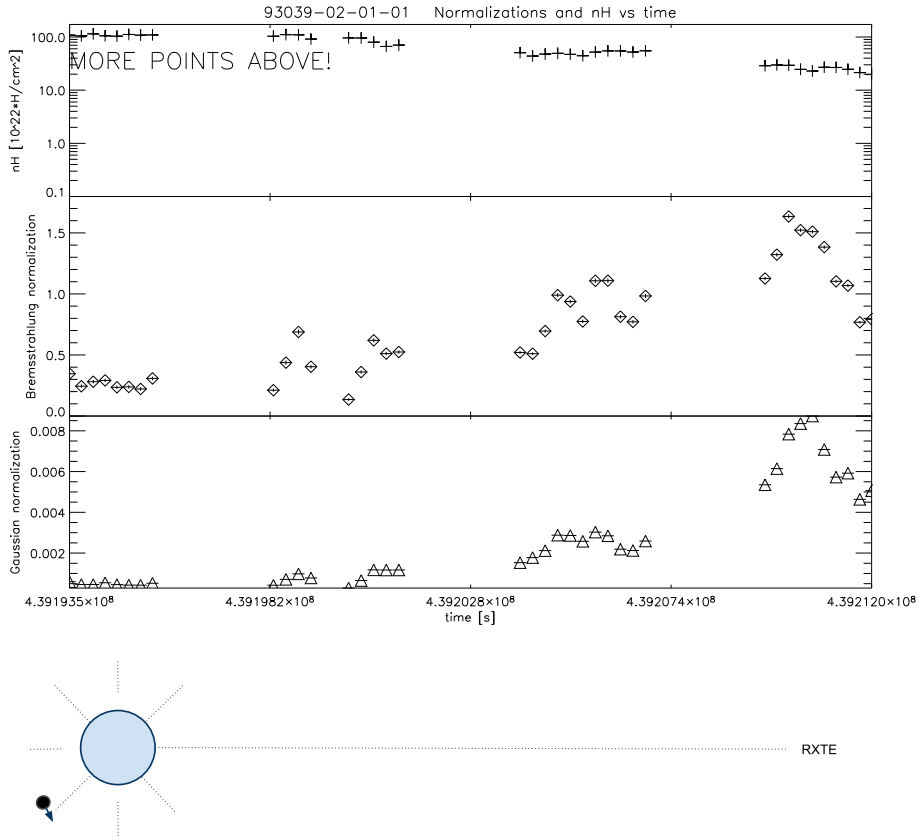

Figure 4.5: Maximum Vela X-1 absorption

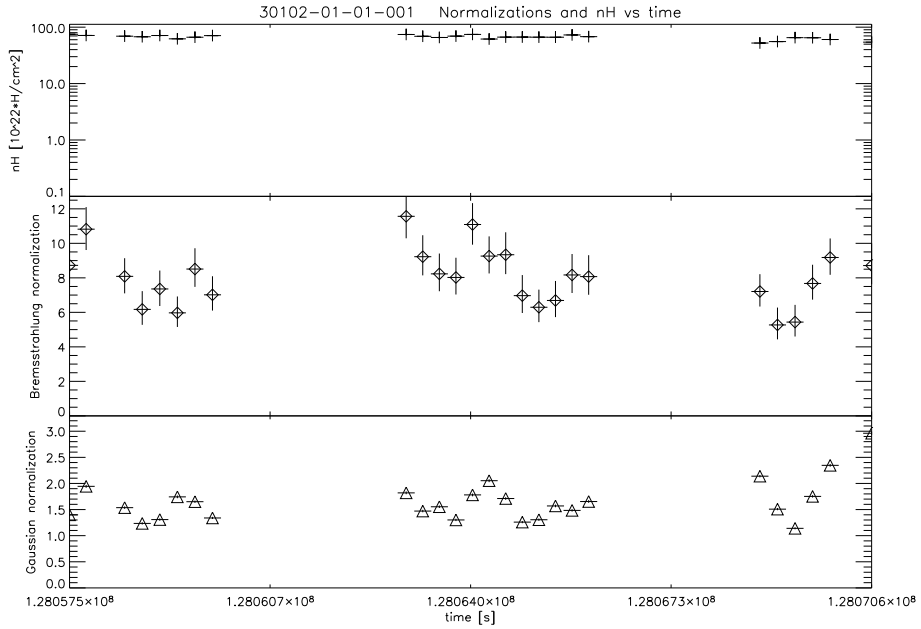

Figure 4.6: Maximum Vela X-1 bremsstrahlung normalization

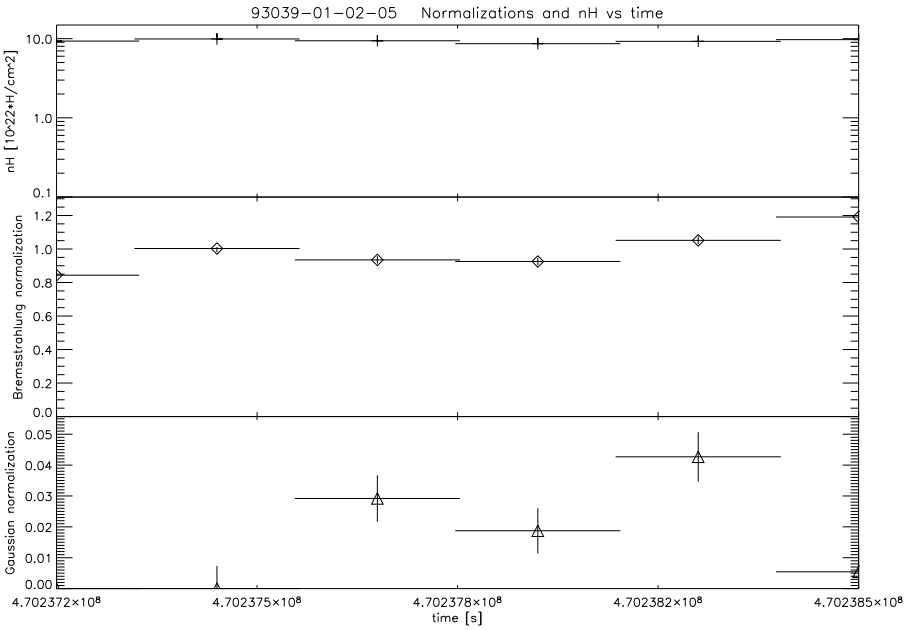

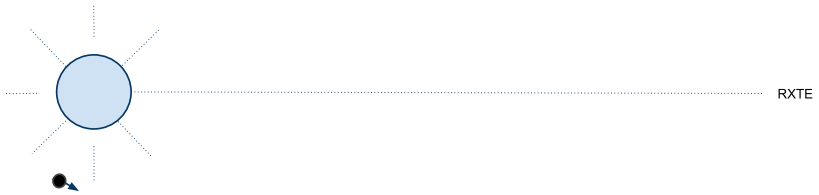

Figure 4.7: Minimum Vela X-1 Gaussian normalization

4.2 Histogram

As in the case of Cygnus X-1, the top histogram in Figure 4.8 has a the number of fits in each bin normalized relative to the entire histogram, while the columns in the lower histogram are each normalized separately. Figure 4.8 shows a very regular absorption dependence on the phase. As a whole, there is significantly more absorption in the second two quadrants of the orbit than in the first two. The isolated pocket of absorption at phase 0.45 was the isolated outburst incident occurring in January of 1998. At approximately phases 0.125 and 0.875 the measured absorption shoots up to a high, but not well defined amount. These phases correspond respectively to the egress and ingress of the neutron star behind the companion star. Fits at phase 0.125 (egress) range from $2.0 * 10^{23} \frac{nH}{cm^2}$ to over $1.0 * 10^{24} \frac{nH}{cm^2}$. The fits seen at ingress (phase 0.875) typically constrained from $4.0 * 10^{23} \frac{nH}{cm^2}$ to $8.0 * 10^{34} \frac{nH}{cm^2}$. The absorption increases by what appears to be a random amount. Notice that there is no data in the phase bin just before the inferior conjunction of the neutron star at approximately phase 0.475.

The due to the limited data set, the correlation data for Vela X-1 are not plotted. The overall Gaussian and absorption data show no interesting correlation behavior. For these plots the center time bins have been removed due to the parameter coupling in the fits at zero time lag. This is because parameter coupling phenomenon may be present here as was discussed in section 2.2.3.

A comparison plot between the bremsstrahlung and Gaussian cross-correlation was carried out here just as was done for the power-law and Gaussian components in Cygnus X-1. For Vela X-1, however, the data bins are too wide for the amount of data we have for the system. This means that there is not enough data for a meaningful correlation between the data sets at lags more than two or three time bins in length. Once again the center time bin of this correlation was removed due to parameter coupling. Within the relevant relevant time bin of approximately 283 seconds there was a positive bremsstrahlung leading correlation of 0.128 and a negative Gaussian leading correlation of -0.65, the rest of the time bins dropped off to negative values for each side of the cross-correlation.

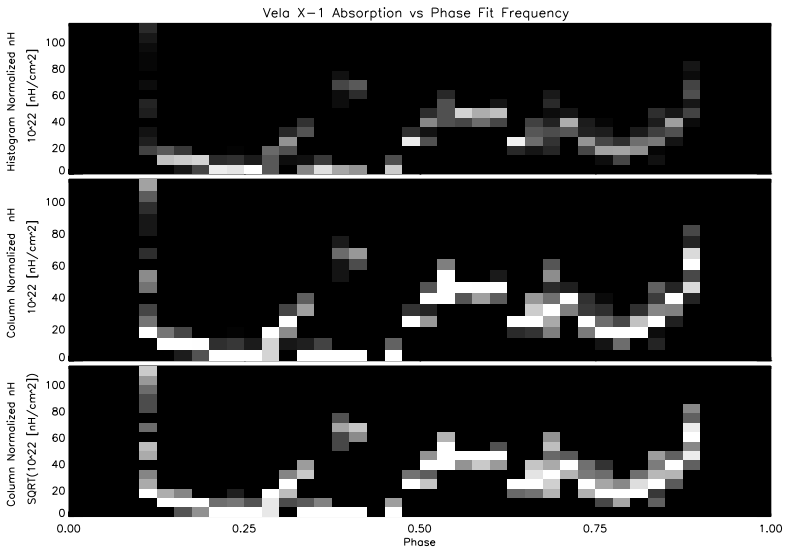

Figure 4.8: Vela X-1 phase-resolved absorption

5 Discussion

5.1 Cygnus X-1

In Cygnus X-1, observations near superior conjunction tend to show higher absorption. This seems plausible since these photons would have to pass through more of the companion's stellar wind and any structures which develop from it. Therefore it would be more likely for the superior conjunction X-rays to be absorbed to some degree. However, we still see a large number of very low fits even at these phases. From this we can conclude that the overall absorption around Cygnus X-1 is sparse, yet increases in the absorption are seen preferentially near superior conjunction of the black hole. In any case, it is very clear that any high absorption structures due to the stellar wind are inconsistent for Cygnus X-1.

The increase in absorption shown in the histogram (Figure 3.8) in the vicinity of phase 0.0 / 1.0 could be the wind of the companion being focused on to the black hole due to its gravitational pull. This could be significant as HDE 226868 is close to filling its Roche lobe (Conti 1978; Gies & Bolton 1986a,b). This effect could increase the density of the stellar wind in the region between the companion and the black hole (Friend & Castor 1982). Theoretically this structure would approach a full Roche lobe overflow geometry as the companion evolves in time because there is a continuum of possible accretion flows that can range between the extreme cases of full wind accretion found in HMXBs and Roche lobe overflow found in LMXBs. My data do not show a significant increase in wind density above $4.0 * 10^{22} \frac{nH}{cm^2}$, but it is possible that this effect consistently increases the

density at lower absorption values. Otherwise, my data do not appear to back up the assertion of a regular focusing of the wind increasing the density. It is possible that the focusing of the wind is not consistent in Cygnus X-1. It is also possible that even if the focused wind did form in Cygnus X-1, it might not obstruct the X-rays from our line of sight due to the system's angle of inclination.

An accretion wake from the black hole passing through the wind of the companion star could be responsible for an increase of lower absorption fits seen around phase 0.75 and higher. However, since the speed of Cygnus X-1's stellar wind is comparable to the orbital speed this would push out such a wake to illuminated at much earlier phases (see Figure 1.2). As mentioned before, at inferior conjunction there generally should be less stellar wind that the X-ray emissions must travel through. While theoretically there could still be significant absorption in this region due to structures created by the regular compression of stellar wind due to the compact object's orbit, this does not seem to be the case for Cygnus X-1. With the exception of a few absorption peaks while the black hole is in egress, my data are consistent only with structures both between the two members of the binary and following the path of the black hole such as tidal streams and focused winds (Friend & Castor 1982; Blondin et al. 1991).

The power-law auto correlation shown in Figure 3.9 falls off slowly. The auto-correlation of the Gaussian normalization has almost no correlation whatsoever. The auto-correlation of the hydrogen absorption starts off slightly correlated and falls off faster than that of the power-law. This means that the time it takes for the typical clump to pass in front of and absorb the system's X-ray emissions is longer than the timescale of typical X-ray flares for that system. The cross-correlations for Cygnus X-1 (Figure 3.10) show an anti-correlation between the absorption measured and the emissions components for small time lags. This appears to be due to the source locally getting dimmer when the absorption increases, as the dimming of the source from our perspective behind the absorption is accounted for in the model. The power-law and Gaussian components are positively correlated with each other. This positive correlation appears to be slightly anti-symmetric around zero time lag.

The asymmetry between the power-law and Gaussian time correlated components shown in Figure 3.11 has significance. Physically, this could mean that power-law photons scattered from the corona of the black hole could be incident on neutral material several seconds of light travel away which then results in X-ray fluorescence of that material. For Cygnus X-1, the distance from the orbiting black hole to the surface of the companion is approximately 10 million km, According to Figure 3.11 there seems to be an echo of the Gaussian component from the power-law. This is the blue line that tends to be higher for first few time bins. This could mean that there are power-law X-rays incident on neutral material that is much further out than the companion itself. This fluorescence could originate from dense stellar wind structures traveling away from the star due to the effect of the orbital bow shock, accretion wake, or the instability of the stellar wind which was discussed before. These are the same structures which can theoretically cause spikes in the X-ray emission or absorption of those X-rays depending on their configuration with the compact object.

What the data actually show is the opposite of what we have predicted. The cross-correlation of the power-law and Gaussian components is actually more symmetric at the inferior conjunction while the data for the superior conjunction shows what appears to be an echo of the Gaussian to the power-law. The reason for this is not clear. It was assumed that the surface of the star should X-ray fluoresce. The surface of the companion to the black hole should correspond to the first 4 to 5 bins in the correlation. However, the correlation comparison for the system in inferior conjunction does not show a echo of the Gaussian to the power-law in this range. If the stellar surface does not effectively fluoresce then my results might be explained as the companion star blocking the backwards traveling radiation from the inferior conjunction while the the same radiation emitted while the black hole is in superior conjunction is incident on gas further back causing the echo seen in Figure 3.13. This remains to be seen however as there is no reason why the surface of the companion should not fluoresce.

The small difference seen between each side of the power-law and Gaussian cross-correlation in Figure 3.13 was analyzed for significance above the noise. The difference between the first 12 bins

of each side of the cross-correlation were compared to the total uncertainty of all 24 points used to compute the difference. It was found that the difference is 0.598 sigma from the error of the data. This means that there is a 27% chance that there is no physical difference between the two sides of the cross correlation and that my result is realized purely by random noise. Therefore I can draw no definitive conclusion as to a fluorescence echo seen in these data. However, the difference is in the expected direction with the power-law component leading the Gaussian. Even if the statistics were better for this calculation, the overall asymmetry of the entire power-law and Gaussian cross-correlation is only 7%. This means that the vast majority of all reflection in the system happens locally within the disk, which is less than a second away from the initial X-ray source and far too short to be seen in my correlation.

5.2 Vela X-1

The wide increase in absorption from approximately phase 0.50 to 0.80 is consistent with a focused wind or accretion wake of material being accreted onto the neutron star. As the neutron star passes its inferior conjunction and heads back into eclipse these structures are brought into the line of sight of Vela X-1's emissions by RXTE. The large amount of absorption on each side of the histogram corresponds to ingress and egress of the neutron star. This is likely due to the corona of the companion star as the neutron star passes behind it causing the X-rays to be highly absorbed from our perspective. This effect could also be caused by the edge of the focused wind. The randomness seen here is likely due to very wide phase bin used. It is possible that the change in absorption values at ingress and egress is smooth, yet so abrupt that within a single phase bin that observations taken within this phase bin consistently saw a huge range of absorption values.

The increasing amount of absorption seen in Figure 4.8 in phases immediately after 0.5 could be evidence of a tidal stream predicted by Blondin et al. (1991). The histogram of my experimental Vela data is consistent with figure 2 given in Blondin et al. for the predicted absorption due to their model of a system similar to Vela X-1.

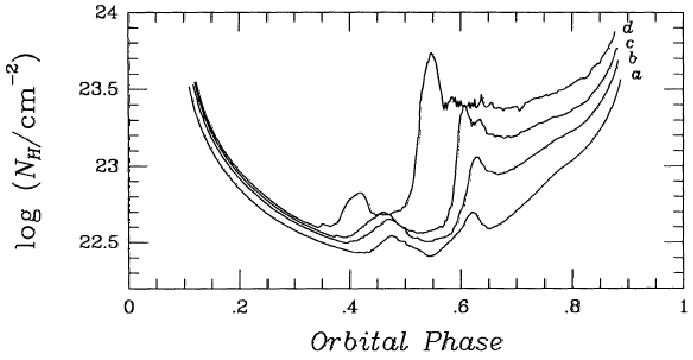

Figure 5.1: Model of HMXB with strong stellar wind (Blondin et al. 1991)

There is no evidence of such a tidal structure in Cygnus X-1. According to Blondin's models, it would occur at earlier phases than a focused wind or accretion wake, but this is not seen in the data. The lack of this structure could simply be due to the height of the orbit of the black hole which is further from out from its companion than its counterpart in Vela X-1, so no stream can be supported. It is also possible that that the inclination angle of Cygnus X-1's orbit is so large that a tidal stream, should it actually be produced, will never be illuminated by the X-rays produced in this system.

Fürst et.al (2010) plot the counts given in the ASM energy channels as well as a crude hardness measure computed from a ratio of these channels. They find that the spectrum of Vela X-1 steadily hardens with the phase. Comparing this with my absorption histogram we see that the increasing absorption with phase due to the accretion wake of the NS can very well account for the hardening of the spectrum that they see. To do this they plot the RXTE ASM data channels as (C-B-A)/(A+B+C). As the counts in the lower energy channels are lessened this causes the ratio to go up as a measure of the hardness of the system.

The asymmetry between the bremsstrahlung and Gaussian radiation components found in the cross-correlation comparison is consistent with a initial bremsstrahlung radiation incident on material which then fluoresces. Due to the quality of our data we can only mention this behavior up to about 283 seconds out from the initial source.

Bibliography

[1] Bolton, C. T. 1972a, Nature 235: 271-73

[2] Bolton, C. T. 1972b, Nature Phys. Sci. 240:124-27

[3] Bolton, C. T. 1975, ApJ 200, 267-77

[4] Bondi, H., & Hoyle, F., 1944, MNRAS, 104, 273

[5] Bowyer, S., Bryam, E. T., Chubb, T. A., & Friedman, H., 1965, Science, 147, 394

[6] Bozzo, E., Falanga, M., Stella, L., 2008, ApJ, 683,1031

[7] Blondin, J. M., Kallman, T. R., Fryxell, B. A., & Taam, R. E., 1990, ApJ, 356, 591

[8] Blondin J.M., Stevens I.R., Kallman T.R., 1991, ApJ 371, 684

[9] Bradt, H. V. D., & McClintock, J. E. 1983, ARA&A, 21, 13

[10] Castor, J. I., Abbott, D. C., & Klein, R. I. 1975, ApJ, 195, 157-174

[11] Chandrasekhar, S., 1943, ApJ, 97, 255

[12] Chodil, G., Mark H., Rodrigues, R., Seward, F. D., & Swift, C. D., 1967, ApJ, 19, 681-683

[13] Coe, M. J., Fabregat, J., Negueruela, I., Roche, P., & Steele, I. A. 1996, 281, 333

[14] Conti, P.S. 1978 A&A, 63, 225

[15] Cowie, L. L., 1977, MNRAS, 180, 491

[16] Forman, W., Jones, C., Tananbaum, H., Gursky, H., Kellogg, E., & Giacconi R. 1973, ApJ (Letters), 182, L103

[17] Friend, D.B., & Castor, J.I. 1982 ApJ, 261, 293

[18] Fürst, F., Kreykenbohm, I., Pottschmidt, K., et al. 2010, AA, 519, A37

[19] Giacconi R., Gursky, H., Paolini, F. R., Rossi, B. B. 1962, Phys. Rev. Lett. 9:439-43

[20] Gies, D.R., & Bolton, C.T. 1986a, ApJ, 304, 371

[21] Gies, D.R., & Bolton, C.T. 1986b, ApJ, 304, 389

[22] Hoyle, F., & Lyttleton, R. A 1939, in Proceedings of the Cambridge Philosophical Society, vol 35,issue 03, p.405

[23] McClintock, J. E., et al. 1976, ApJ (Letters), 175, L19

[24] McClintock, J. E., & Remillard, R. A 2003, arXiv:astro-ph/0306213

[25] Negueruela I., Smith D.M., Reig P., Chaty, S., & Torrejn, J. M., 2006, In:Wilson A. (ed.) Proceedings of the The X-ray Universe 2005, Madrid, ESA-SP 604., Noordwijk: ESA

[26] Romano, P., La Parola V., Vercellone, S., Cusumano, G., Sidoli, L., Krimm H. A., Pagan, C., Esposito, P., Hoversten, E. A., Kennea, J. A., Page K. L., Burrows, D. N., Gehrels, N., 2010, MNRAS, 410, 3, 1825-1836

[27] Shakura N. I., & Sunyaev R. A., 1973, Astr. and Ap., 24,337

[28] Shapiro S. L., Lightman A. P., Eardley D. M., 1976, ApJ, 204, 187

[29] Smith, D. M., Negueruela, I., Pottschmidt, K., Markwardt, C. B., Bezayiff, N., 2006, American Astronomical Society, HEAD meeting #9, #1.77; Bulletin of the American Astronomical Society, Vol. 38, p.341

[30] Smith, D. M., Heindl, W. A., Swank, J. H., Harrison, T. E., & Negueruela, I., 2003, ATel, 182

[31] Smith, D.M., Main, D., Marshall, F., et al., 1998, ApJL, 501, L181

[32] Stella, L., & Rosner, R. 1984, ApJ, 277, 312

[33] Taam, R. E., Fu, A., & Fryxell, B. A., 1991, ApJ, 371, 696

[34] Theuns, T., Boffin, H. M. J., & Jorissen, A., 1996, MNRAS, 280, 1264

[35] Owocki, S. P., Castor, J. I., Rybicki, G. B., 1988, ApJ, vol. 335, p. 914-930.

[36] Owocki, S. P.; Rybicki, G. B, 1984, ApJ, 287, 337-350

[37] S. Yamauchi, T. Aoki, K. Hayashida, et al., 1995, PASJ, 47, 189

[38] , B. L., Murdin, P. 1972 Nature 235:37-38